Kaunas University of Technology

Faculty of Mechanical Engineering and Design

Fabrication and Characterization of PVDF/$BaTiO_3$ 3D Printing Material

Master's Final Degree Project

Sotirios Alexandridis

Project author

Assoc. Prof. Marius Rimašauskas

Supervisor

Kaunas, 2022

Kaunas University of Technology

Faculty of Mechanical Engineering and Design

Fabrication and Characterization of PVDF/$BaTiO_3$ 3D Printing Material

Master's Final Degree Project

Mechatronics (6211EX017)

Sotirios Alexandridis

Project author

Assoc. Prof. Marius Rimašauskas

Supervisor

Lect. Darius Eidukynas

Reviewer

Kaunas, 2022

Kaunas University of Technology

Faculty of Mechanical Engineering and Design

Sotirios Alexandridis

Fabrication and Characterization of PVDF/$BaTiO_3$ 3D Printing Material

Declaration of Academic Integrity

I confirm the following:

1. I have prepared the final degree project independently and honestly without any violations of the copyrights or other rights of others, following the provisions of the Law on Copyrights and Related Rights of the Republic of Lithuania, the Regulations on the Management and Transfer of Intellectual Property of Kaunas University of Technology (hereinafter – University) and the ethical requirements stipulated by the Code of Academic Ethics of the University;

2. All the data and research results provided in the final degree project are correct and obtained legally; none of the parts of this project are plagiarised from any printed or electronic sources; all the quotations and references provided in the text of the final degree project are indicated in the list of references;

3. I have not paid anyone any monetary funds for the final degree project or the parts thereof unless required by the law;

4. I understand that in the case of any discovery of the fact of dishonesty or violation of any rights of others, the academic penalties will be imposed on me under the procedure applied at the University; I will be expelled from the University and my final degree project can be submitted to the Office of the Ombudsperson for Academic Ethics and Procedures in the examination of a possible violation of academic ethics.

Sotirios Alexandridis

Confirmed electronically

Kaunas University of Technology

Faculty of Mechanical Engineering and Design

Task of the Master's final degree project

Given to the student – Sotirios Alexandridis

1. Title of the project

Fabrication and Characterization of PVDF/$BaTiO_3$ 3D Printing Material

(In English)

PVDF/$BaTiO_3$ 3D spausdinimo medžiagos gamyba ir savybių vertinimas

(In Lithuanian)

2. Hypothesis

Melt-extruded PVDF/$BaTiO_3$ composite filament with consistent dimensions and even particle distribution can be utilized for FDM 3D printing with reduced clogging probability and stable operation.

3. Aim and tasks of the project

Aim: to investigate properties and printability of PVDF/$BaTiO_3$ composite 3D printing material

Tasks:

1. to fabricate 3D printing material with $BaTiO_3$ ceramic particles inclusions;
2. to determine main quality parameters of produced filament;
3. to evaluate printing properties and identify main printing parameters;

4. Initial data of the project

N/A

5. Main requirements and conditions

- 1.75mm filament fabrication with Noztek extruder and puller-winder system
- Slicing on PrusaSlicer 2.4 and 3D printing on direct extruder Prusa i3 MK3S
- Tensile testing of type 1B specimen as per ISO 527-2

Project author	Sotirios Alexandridis		2022.02.28
	(Name, Surname)	*(Signature)*	*(Date)*
Supervisor	Marius Rimašauskas		2022.02.28
	(Name, Surname)	*(Signature)*	*(Date)*
Head of study field programs	Regita Bendikienė		2022.02.28
	(Name, Surname)	*(Signature)*	*(Date)*

Alexandridis, Sotirios. Fabrication and Characterization of PVDF/$BaTiO_3$ 3D Printing Material. Master's Final Degree Project, supervisor Assoc. Prof., Marius Rimašauskas; Faculty of Mechanical Engineering and Design, Kaunas University of Technology.

Study field and area (study field group): Production and Manufacturing Engineering (E10), Engineering Sciences (E).

Keywords: additive manufacturing, polyvinylidene fluoride, barium titanate, filament extrusion, nanocomposite

Kaunas, 2022. 59 p.

Summary

During this work a polyvinylidene fluoride / barium titanate composite 3D printing filament was fabricated, with target diameter 1.75mm and accuracy of ±0.1mm. The used equipment included a desktop filament extrusion machine (Noztek Touch), a cooling fan array and a pulling system. It was found that accurate filament diameter could be obtained by using an oversized die of 2.75mm and, with the use of adjustable pulling speed, obtain the correct diameter. Special attention was given to the pulling system electronics, the stepper driver controller was redesigned and control software was developed for fine and precise control. The extruder was tested with polylactic acid pellets and PVDF/ $BaTiO_3$ pellets and powder to produce pure PLA filament, pure PVDF filament and PVDF/ $BaTiO_3$ filament of 3wt% and 9wt% concentration. Extruder temperature was stair stepped at 235°C and 225°C and speed was maintained stable at 25 RPM. It was determined that pelletizing and remelting the produced filament resulted in better material flowability and processability through the extruder and more stable diameter was achieved. The mean diameter value for 9wt% PVDF/ $BaTiO_3$ filament was 1.82mm, with process capability indices of Cp=2.6 and Cpk=0.67. The produced PVDF filament was used in a Prusa i3 MK3S+ FDM printer. No obstruction of the nozzle of 0.4mm was observed while printing at 250°C. A heated bed and Dimafix adhesive were used to aid bed adhesion and prevent warping. Fully 3D printed specimen was not obtained due to blob artifacts on the print surface, which eventually resulted in excessive accumulation of material on the nozzle tip and prevented interlayer bonding.

Alexandridis, Sotirios. PVDF/$BaTiO_3$ 3D spausdinimo medžiagos gamyba ir savybių vertinimas. Magistro baigiamasis projektas, vadovas doc. Marius Rimašauskas; Kauno technologijos universitetas, Mechanikos inžinerijos ir dizaino fakultetas.

Studijų kryptis ir sritis (studijų krypčių grupė): Gamybos inžinerija (E10), Inžinerijos mokslai (E).

Reikšminiai žodžiai: adityvi gamyba, polivinilidenfluoridas, barrio titanatas, gijos ekstruzija, nano kompozitai

Kaunas, 2022. 59 p.

Santrauka

Šio darbo metu polivinilidenfluorido ir barrio titanato kompozitinė gija 3D spausdinimui buvo pagaminta, kurios skersmuo yra 1.75 mm o leistinos nuokrypos ±0.1mm. Tyrimo metu buvo naudota įvairi įranga: „Noztek Touch“ gamintojo stalinis ekstruzijos įrenginys, gijos tempimo įrenginys, o aušinimui buvo naudoti ventiliatoriai. Buvo nustatyta, kad reikalaujamo skersmens 3D spausdinimo gija gali būti pagaminta naudojant didesnio skersmens 2.85 mm ekstrudavimo antgalį, tačiau kontroliuojant gijos ištempimo greitį. Norint užtikrinti tolygų tempimo greitį papildomai buvo modifikuotas tempimo įrenginio žingsninio variklio valdymo blokas ir sukurta nauja valdymo programa. Parengta ekstrudavimo įranga buvo ištestuota su PLA ir PVDF medžiaga, taip pat su skirtingų koncentracijų 3wt% ir 9wt% PVDF/ BaTiO3 kompozitu. Eksperimento metu ekstruderio temperatūra atskirose zonose buvo 235°C ir 225°C tuo tarpu tempimo greitis buvo pastovus ir siekė 25 apsisukimus per minutę. Buvo nustatyta, kad pakartotinas 3D spausdinimo gijos susmulkinimas į granules ir ekstrudavimas leidžia pasiekti geresnių gijos skersmens rezultatų dėl pastovesnio medžiagos tekėjimo, kuris pagerėja dėl sumažėjusio ekstruduojamų granulių dydžio. PVDF/ BaTiO3 9wt% koncentracijos gijos skersmens vidurkis yra 1.82 mm, tuo tarpu proceso galimybių rodikliai Cp=2.6 ir Cpk=0.67. Pagaminta 3D spausdinimo medžiaga buvo naudota su Prusa i3 MK3S+ spausdintuvu. Spausdinimo metu buvo naudotas 0,4 mm spausdinimo antgalis, kurio užsikimšimo nebuvo pastebėta kai spausdinimas buvo atliekamas 250°C temperatūroje. Kaitinama platforma ir klijai Dimafix buvo naudoti norint sumažinti spausdinamo objekto deformacijas. Visiškai atspausdinti bandinius nepavyko dėl medžiagos kaupimosi ant spausdinimo antgalio ir nepakankamos tarpsluoksninės adhezijos.

Table of contents

List of figures

List of tables

List of abbreviations and terms

Abbreviations:

AM – Additive Manufacturing;

FDM – Fused Deposition Modelling;

FFF – Fused Filament Fabrication;

PVDF – Polyvinylidene fluoride;

$BaTiO_3$ – Barium titanate.

DIW – Direct Ink Writing

Terms:

Slicing – Slicing is the process of converting a 3D object into G-code using a piece of software called "slicer".

Bowden system – The 3D printer extrusion system where the extruder is located on the printer's frame and the filament is fed to the hotend through a guiding tube (Bowden tube).

Hotend – The 3D printer component which melts the filament.

Introduction

This written work investigates the fabrication and characterization of a novel 3D printing filament composed of a polyvinylidene fluoride (PVDF) base and reinforced with barium titanate ($BaTiO_3$) particles. PVDF attracts increasing scientific attention due to its unique chemical, thermal properties and its biocompatibility. $BaTiO_3$ has recently been presented as lead-free ceramic additive capable of improving the inherent piezoelectricity of PVDF. A need to rapidly prototype new piezoelectric devices with these nanocomposite materials is evident and additive manufacturing is among the most appropriate fabricating techniques for this purpose.

Firstly, PVDF and PVDF-based composites are presented and their main characteristics, fabrication and testing techniques are reviewed (Section 2).

For the methodological part, this paper mainly focuses on the procedure and process parameters of effectively fabricating a dimensionally accurate PVDF/$BaTiO_3$ filament of various concentration (Section 3). A desktop filament extruder alongside a cooling and pulling system are utilized. Special attention is given to the control parameters of the system and efforts are focused in improving their controllability. Also, waste reduction is explored by considering recycling possibilities of a less than optimal product.

FDM 3D printing properties and parameters are detailed in an effort to determine the optimal settings to successfully obtain PVDF/ $BaTiO_3$ specimens using the filament material (Section 4).

The conclusions of the experimental work are finally formulated and recommendations for improvements, further development, refinement and validation of the procedure are outlined.

Aim: to investigate properties and printability of PVDF/$BaTiO_3$ composite 3D printing material.

Tasks:

1. to fabricate 3D printing material with $BaTiO_3$ ceramic particles inclusions;
2. to determine main quality parameters of produced filament;
3. to evaluate printing properties and identify main printing parameters;

1. Relevance and Novelty

1.1. Project Relevance

Over the past years there is growing scientific attention in novel electroactive polymer and ceramic compounds for biosensor and energy harvesting applications. A broadly studied material is the fluoropolymer polyvinylidene fluoride (PVDF) and it is commonly referred to as a "smart" bioengineering material [1]. The current trend is to develop programmable processes to quickly and efficiently process these new materials. Additive manufacturing (AM) technologies fit these criteria exceptionally well, enabling rapid prototyping and production of geometrically complex objects. AM is already widely used to create bespoke sensing devices, such as various biosensors, wearable devices and energy harvesters [2]. Therefore, it is logical to see AM utilized for the emerging PVDF compounds as well. Indeed, a search on the Web of Science database reveals that the term "PVDF" is increasingly appearing on scientific article topics and citations. Similar trend is observed when the term is combined with "3D printing" (Fig. 1 and Fig. 2).

Recent attempts have proven that 3D printing of PVDF can be achieved via relatively simple means. It has been shown that PVDF pellets can be extruded into filaments compatible with commercially available 3D printers and effectively printed [3, 4].

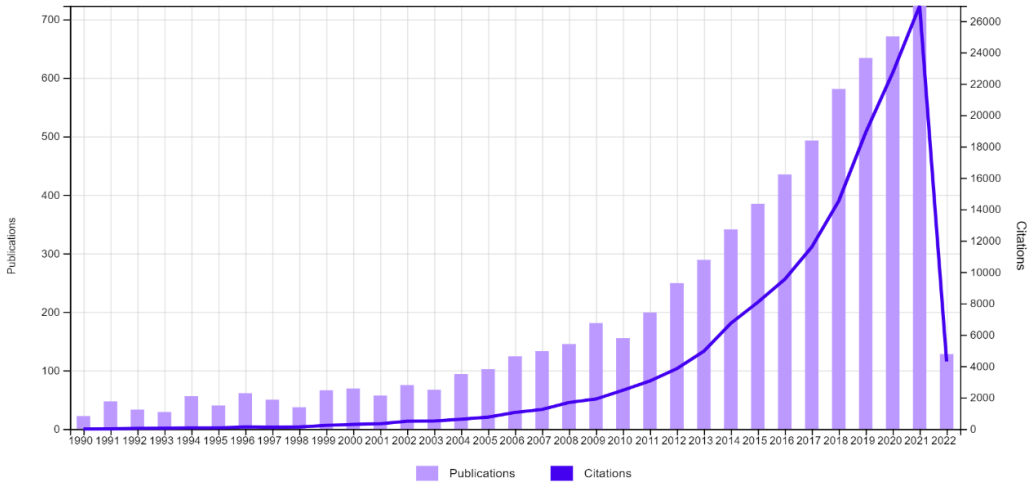

Fig. 1. Trend of scientific publications pertinent to the term "PVDF" [5]

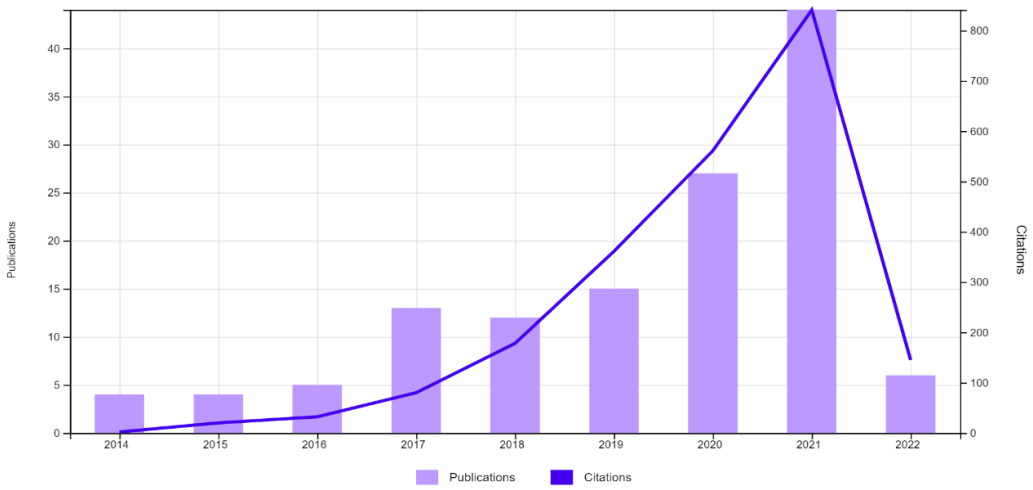

Fig. 2. Trend of scientific publications pertinent to combined terms "PVDF" + "3D printing" [5]

Now, the focus shifts to introducing inclusions which can enhance the piezoelectric properties of PVDF. Barium titanate or $BaTiO_3$ is a high-runner in this respect, since it is environmentally friendly and contains no lead, as more traditional compounds do [6]. This makes it suitable for biomedical applications. Therefore, PVDF/$BaTiO_3$ nanocomposites and their manufacturability via 3D or 4D printing are prominent scientific topics [6, 7, 8]. Of particular interest is the raw material form and the specifif AM technique employed. Fused deposition modeling (FDM) and PVFD/ $BaTiO_3$ filament stock material is presented as a viable fabrication method capable of achieving good distribution of $BaTiO_3$ particles within the PVDF matrix and resulting in bodies with piezoelectric response [8].

Overall, while research of 3D printing of PVDF/ $BaTiO_3$ filaments is still in its infancy, it is evident that there is real prospect which is gradually revealed by ongoing scientific efforts. Consequently, it is worthwhile adapting elements of the research and further optimizing the process, refining technological parameters and investigating the properties of fabricated objects.

1.2. Project Novelty

With the advance of 3D printing technology, an increasing number of specialty filament compositions emerges. New, high-performance materials are already commercially available and more compositions are researched for use in conventional FDM systems. Recent research focuses on raw materials with unique mechanical and electrical properties, such as the PVDF/$BaTiO_3$ nanocomposite. In past research, this nanocomposite was created in filament form, as the stock material for FDM 3D printers. However, the techniques employed for the filament fabrication involved complex, multi-step processes and used solvents to dissolve the PVDF and achieve even distribution of the ceramic particles within the matrix [6, 9]. This poses significant health and environmental risks. Furthermore, it calls for special lab equipment and precautionary measures; factors that further impede the production of such filament in either small or large scale. This translates in higher cost, time and complexity.

In fact, PVDF filaments have been explored in previous research, but no significant attention was given to the fabrication method nor the possibility of incorporating ceramic inclusions. Also, these cases appear to mainly focus on manipulating the printing parameters using software, while the hardware remained at its default manufacturer configuration [4, 10]. Especially case [10] presents a potentially major shortcoming, which is the option of a Bowden extruder 3D printer, which could explain the poor surface quality and difficulty in attaining the multilayer test specimens. On the other hand, case [4] employed a direct extruder, but achieving thin films and exploring their piezoactivity were prioritized.

Literature that focuses on the PVDF/$BaTiO_3$ nanocomposites is more limited. In their article Phatharapeetranun et al. show how $BaTiO_3$ fibers can be mixed with PVDF into a nanohybrid solution that can be processed via a method similar to robocasting, by using a syringe attachment to a desktop 3D printer [9]. While their technique presents promising results in developing composite bodies of high dielectric constant, the stock material fabrication and 3D printing processes are highly complex, they required multiple steps of electrospinning, chemical solutions, thermal treatment and precise control of the technological parameters. Chemical solutions were also used by another research team [6], which succeeded in creating 3D printing filament of 2.89mm in diameter. The volatile and toxic solvent N-dimethylformamide (DMF) used to dissolve the PVDF component of the filament introduces environmental concerns. Hardware modification were performed in this case, however

they aimed to implement in-situ poling, rather than improve the feeding of the filament. Thus, again only thin film specimens are presented.

This research project proposes a straightforward approach for the production of PVDF/$BaTiO_3$ filament. By simple mechanical mixing of PVDF pellets and $BaTiO_3$ powder, filaments of 1.75mm in diameter can be produced with readily available, desktop filament extrusion systems. This is a significant advantage over other research, due to the practicality of this process. The process is quick to set up, involves no harmful compounds, it is low in cost and can be adopted in existing filament extrusion systems with low effort. Also, a direct extruder is suggested as the best option, due to increased extrusion force, better accuracy and control of the stock material feeding to the heated nozzle.

2. Literature Review

This chapter is dedicated to analyzing existing literature pertinent to fabrication of 3D printing filaments, their processing through FDM 3D printing and testing / validation methods for the mechanical properties of 3D printed structures. The aim is to determine the engineering methods employed by other researchers to achieve geometrically consistent filaments and how they tackled potential clogging of the 3D printing nozzle and adhesion issues. Also, the literature review can reveal what are the main contributing factors to extrusion problems, how to detect them and what methods should be used to evaluate the finished product.

As a first step, it is necessary to familiarize with the properties and applications of the materials used for the experimental work. Then, the 3D printing stock material fabrication methods are investigated. A general overview of the typical filament fabrication techniques and utilized equipment is presented. Particular focus is given to the analysis of specialty filament fabrication, so to determine which are the most critical process parameters and what special conditions apply for materials like fluoropolymers. The next step is to explore past attempts of 3D printing this type of filaments, with the emphasis on the used equipment and the effects of different settings on the printability. Lastly, the testing methods applicable for 3D printed parts are researched and the testing results are evaluated.

2.1. Materials Introduction

2.1.1. PVDF

Polyvinylidene fluoride or PVDF belongs to the thermoplastic family of fluoropolymers, among other polymers like polytetrafluoroethylene (PTFE or Teflon®). It is marketed under a number of brand names, the most popular of which are Kynar® and Solef® [11, 12]. It is characterized by superior chemical, thermal and UV resistance and sterilizability. These attributes make it a good candidate for the use in harsh environments (e.g. as pipes or fittings) and in advanced biomedical applications [13, 14].

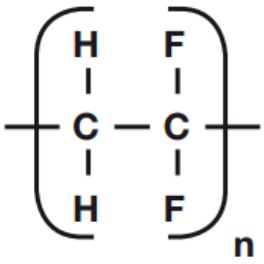

Fig. 3. PVDF monomer chemical formula [12]

PVDF is produced by polymerizing vinylidene difluoride (VDF) monomers into long chains. It can either be processed into a homopolymer or a copolymer with hexafluoropropylene (PVDF-HFP), chlorotrifluoroethylene (PVDF-CTFE) or tetrafluoroethylene (PVDF-TFE). The PVDF molecular chains can be arranged in at least 4 crystalline structures or phases (Fig. 4) [15]:

- α: the default form in melt processing
- β: forms under mechanical stretching in high temperature
- γ: forms under special circumstances, by transitioning from β-phase, or directly form α-phase
- δ: forms under distortion and application of high electric fields

The β-phase is of particular interest, because PVDF exhibits strong piezoelectric behavior at this crystalline structure. Films made of PVDF transitioned to β-phase are used for energy harvesting applications and can be integrated into ultrasonic transducers, audio transducers, medical transducers, display devices, vibrometers, shock sensors and pressure sensors. The electroactivity of PVDF depends on the alignment of molecular dipoles. At β-phase the dipoles are aligned parallel to each other resulting in a high dipole moment. PVDF-TFE is of particular interest, because it directly attains the polar phase, without the need of transitioning from the α-phase [16]. β-phase transformation can be achieved by stretching PVDF parts and polling with the application of a high electric field. Poling processed include contact poling, corona poling and electrospinning [3].

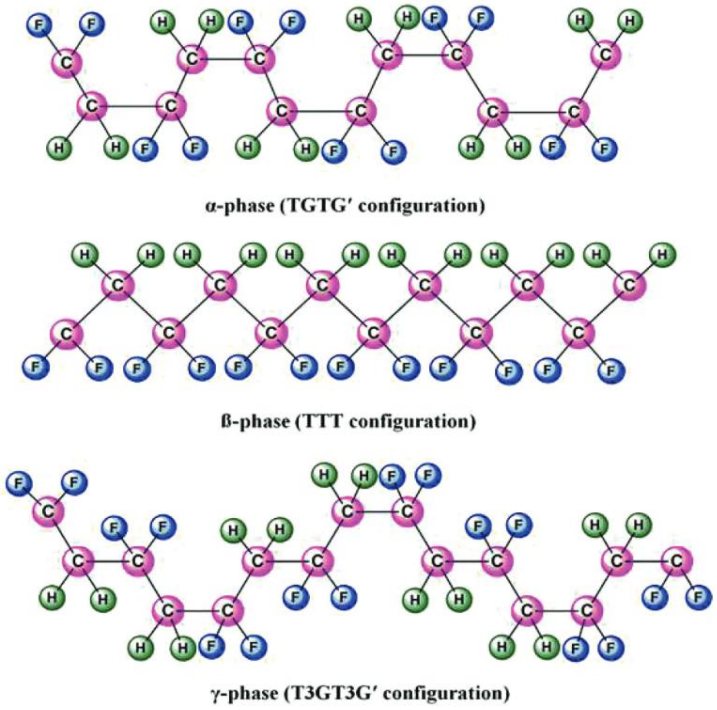

Fig. 4. The 3 first crystalline phases of PVDF [16]

The applications areas of PVDF are quite wide. For its high-performance characteristics, it is an excellent material for replacing metal counterparts in high purity applications. Such examples are valves, pumps, fittings, vessels, nozzles or tubing in fluid handling systems, where corrosive chemicals or high temperature compounds are involved. Because it is non-reactive with most chemical compounds and also sterile, it is also appropriate for use in the food and pharmaceutical industry, compliant with the relevant industry standards. In fact, there is only a limited amount of chemicals in which PVDF is soluble in. Some common solvents are methyl ethyl ketone (Butanone), dimethyl formamide (DMF) and N-Methyl-2-pyrrolidone (NMP). It is fire resistant and retardant with a rating of 150°C and it is a good electrical insulator, thus it is used as wire and cable sheathing and can be processed as a binder for batteries for the automotive industry. It can also be applied as surface paint or coating in architecture, providing weather protection [17].

PVDF copolymers are generally regarded as more favorable, due to the flexibility to very the copolymer content and therefore attain different properties, according to the application [18]. Copolymer additives decrease the PVDF crystallinity and result in a softer product, which is easier to process with conventional fabrication techniques, like injection molding. A very popular PVDF copolymer is the PVDF Flex ® developed by Arkema, which comes in different grades. Its exact

formulation is patented by Arkema and, as the brand name suggests, features great flexibility, but also high tensile strength up to 55MPa over a wide temperature range [17, 18]. Additionally, PVDF resins advertised under the Kynar name can be recycled multiple times without degradation.

As mentioned above, PVDF exhibits the most intense piezoelectric behavior at its β-phase polymorph. There is a number of techniques of achieving the transition. Zerun et al. describe PVDF film formation via spin-coating technique and via the Langmuir–Blodgett (LB) Deposition method [19]. The preparation of the PVDF solution for spin-coating is summarized in Fig. 5. Initially, PVDF is dissolved in an organic polar solvent and homogenized using a magnetic stir bar. Then the solution is poured on the spin-coating apparatus. Parameters like temperature, spinning speed and humidity influence the formation of the crystalline structure, with higher temperatures (>40°C) promoting the β-phase crystallization, especially if combined with high spinning speed and low solvent concentration. A final annealing step is carried out to improve the film's morphology and prevent the formation of porous structures. Additional post processing actions can be performed, like stretching and electrical poling, to further enhance the dipole alignment. Spin-coating can achieve relatively thick PVDF films of a few tens to a few thousand nanometers.

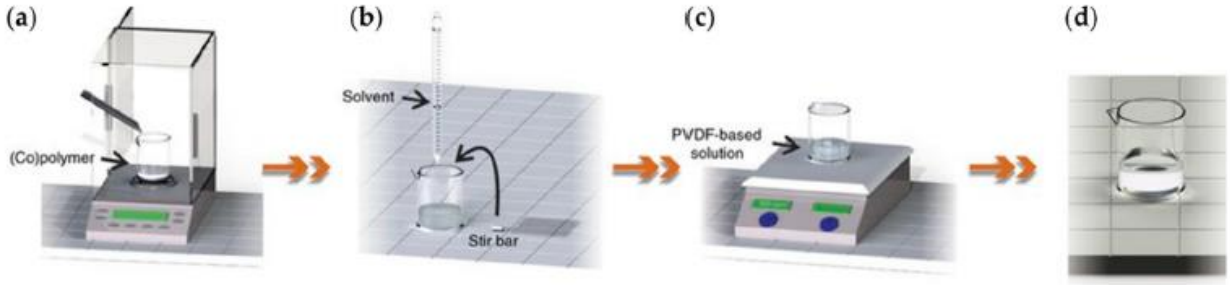

Fig. 5. PVDF thin film preparation via spin-coating [20]

The LD Deposition is the preferred method for obtaining ultra-thin or two-dimensional films, with a thickness of only a few nanometers. First, PVDF is formed into an acetone or a dimethyl sulfoxide (DMSO) solution, which lends amphiphilic properties to the compound. This solution can be then spread on water. Next, the floating molecules are compressed to and deposited on a surface (Fig. 6). The films transferred on the substrate can be 2-3nm thick, with thicker samples being possible by successively depositing several layers. The final step is annealing at 120°C.

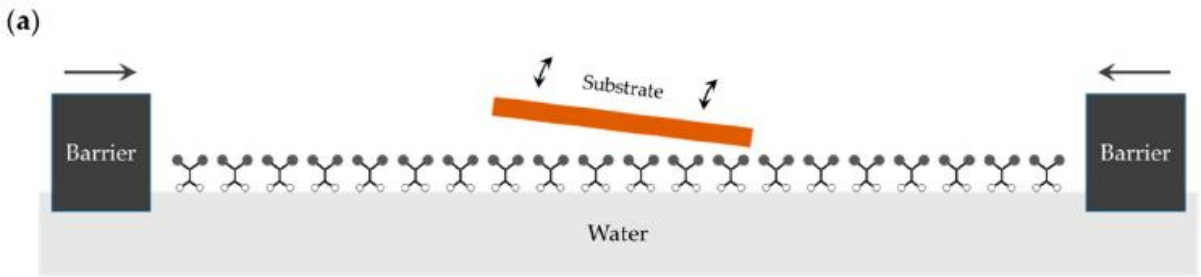

Fig. 6. Langmuir–Blodgett Deposition for PVDF thin films [19]

2.1.2. PVDF Composites

While PVDF can be piezoelectric by itself, research reveals a clear trend of further promoting the piezoelectric properties by introducing fillers in the PVDF matrix. These fillers fall in one of the

following categories: ceramic, carbon-based, metal-based, hybrid and bio-based. The general aim and outcome of these composite formulations is the enhancement of the piezoelectric properties of PVDF.

Ceramic Fillers

Ceramic fillers have drawn immense scientific attention recently. Ceramics are inorganic compounds of metal, non-metal or metalloid atoms. The most prominent ceramic formulations compounded in PVDF are lead-zirconate-titanate (PZT), barium titanate (BaTiO3), sodium potassium niobate (KNN) and bismuth sodium titanate (BNT) [16].

PZT in PVDF was researched in composites of 50vol% and it was found that the PZT particle size influences the piezoelectric coefficient of the material, with larger particles promoting an increase of the β-phase component in the composite [21]. Similar findings are reported in PVDF-PZT films with different concentrations (up to 30vol%), produced via solution casting. The results mention a 75% increase of the β-phase content, but also improved piezo-strain constant d_{33} of 84 pC/N, at the highest PZT concentration [22]. Despite its piezoelectric enhancing properties, PZT is often regarded as an unfavorable additive due to its difficult processing and lead content.

Therefore, researchers turn their focus to lead-free ceramics, with $BaTiO_3$ being a very popular option. Barium titanate (abbreviated as BaTiO3 or $BaTiO_3$) is a ferroelectric ceramic with high dielectric constant. Due to its excellent piezoelectric properties, it is often used to reinforce polymer matrices and enhance their piezoactivity [8, 16]. It has been shown that a novel PVDF/$BaTiO_3$ composite sheet with calcinated $BaTiO_3$ powders have improved electrical properties. The powder is calcinated at high temperature with piezoelectric constant of 166.38 and strain constant of 25 pC/N [23]. PVDF-TrFE copolymer has also been tested in nanocomposites with $BaTiO_3$ and processed into films, as dopant in carbon nanotubes. The findings again showed improved dielectric constant at 1KHz and a concentration of approximately 11vol% of PVDF-TrFE/PZT with the nanotube film [24]. The drawbacks of ceramic fillers are their brittle nature, they are non-ductile and complex processes are required for their shaping and overall processing [16].

Carbon-based Fillers

Carbon-based fillers reinforce the PVDF matrix by lending properties like high stiffness, low density and good electrical and thermal conductivity. Such fillers are carbon nanotubes (CNT) and graphene oxide (GO) [16]. The advantages of CNT inclusion are underlined by Kim et. al, with their results showing that CNT can lead to better dielectric parameters, with relatively lower polling voltages [25].

Another comparative study explored the piezoelectric characteristics of PVDF/CNT and iron-reduced graphene oxide (Fe-RGO)/PVDF nanocomposite films for energy harvesters. The output voltage and current of the CNT film were reported to be higher than the Fe-RGO film, with open circuit measurements reaching 2.5V and 700nA respectively [26].

Metal-based Fillers

Metallic fillers like zinc oxide (ZnO) and silver (Ag) can enhance the piezoelectric response of PVDF, while allowing for flexible structures, with high tensile strength and thermal stability [16]. Such examples are PVDF-TrFE/ZnO nanowires, where the ZnO aimed to extend the β-phase crystallinity of the PVDF matrix. The silver fillers were prepared by a polyol technique and then incorporated into

the PVDF, which was first dissolved in N-Methyl-2-pyrrolidone. After a poling step, the nanowires were aligned, which lead to a fourfold increase of the dielectric constant [27].

Hybrid Fillers

They generally include two components, one organic and one inorganic. Examples of hybrid fillers include rGO/ZnO and TiO_2/MWCNT. It was shown that hybrid fillers help achieve composited of higher piezoelectric coefficient by increasing β-phase content to 80% or more. Also, it was estimated that hybrid filler loading can be reduced, making the PVDF doping process more cost effective and less complex [16].

Bio-based Fillers

They are used for the fabrication of biopolymer composites. They were explored as a solution for biocompatible energy harvesters. Deoxyribonucleic acid (DNA) has been used to promote the β-phase nucleation and align the PVDF dipoles. Thin films produced had an 80% β-phase content and they were utilized as nanogenerators with output voltage of 6V and current of 88nA [28]. Another biopolymer consisted of folic acid doped PVDF films with β-phase content of 71.4% and dielectric constant of 218 [29].

2.2. 3D Printing and Poling of PVDF-based Materials

Attempts to process PVDF and its composites by 3D printing begin with the preparation of the stock material. The form of the stock material depends on the particular 3D printing technology employed. This section explores these different types of stock materials and their fabrication techniques.

Direct Ink Writing

Chen et. al present a 3D printing technique based on Direct Ink Writing (DIW) or Robocasting to produce thin films of PVDF films reinforced with multi-walled carbon nanotubes (MWCNTs) and graphene (GR). The printing medium was prepared in a liquid ink form, which was deposited in several layers in a linear, alternating raster on a copper sheet, over a heated surface. The purpose of the copper sheet was to act as an electrode, while high voltage was applied to the syringe's metal tip, effectively achieving in-situ poling. The heated surface evaporated the solvent during printing. The top and bottom layer were finally then painted with a conductive gold layer, which served as an electrode to test the films electrical output. The resulting film was approximately 70μm in thickness. The process is summarized in Fig. 7.

The 3D printed sample was compared against a film produced by simply dissolving PVDF, spreading the solution over a surface and allowing the solvent to evaporate. The aim was to observe the effect of in-situ poling and doping on the β-phase transformation of the PVDF. The results indicated that a higher PVDF concentration ink promoted the α to β phase transition. Crystallinity was also strongly increased by the addition of nucleation agents, with GR resulting in output voltage twice as high as in MWCNT reinforced PVDF. The GR better performance was attributed to its lamellar structure and it was theorized that it induced electric fields which interact with the PVDF molecular structure [30].

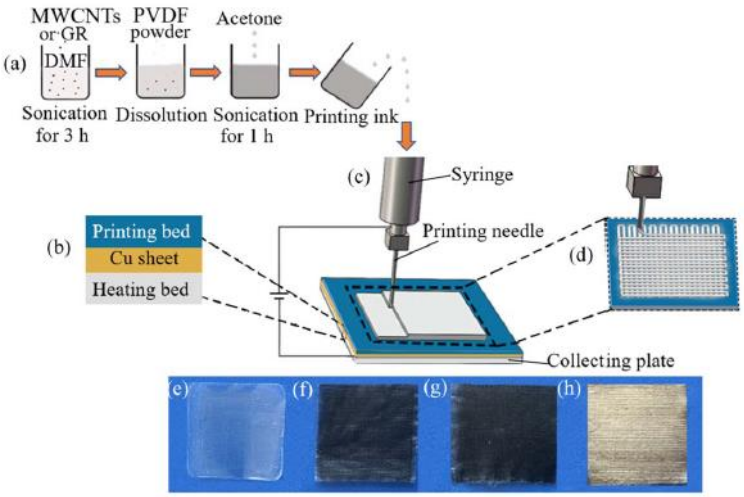

Fig. 7. Preparation of PVDF/MWCNT and PVDF/GR inks (a), DIW printing process (b-d), and resulting films: pure PVDF (e), PVDF/MWCNT (f), PVDF/GR (g), film with electrodes (h) [30]

A similar technique was explored by Phatharapeetranun et. al, but this time the nanocomposite consisted of PVDF mixed with electrospun $BaTiO_3$ nanofibers (BTNFs) in ink form. A number of testing techniques were used to evaluate the printed sampled. X-ray crystallography (XRD) was used to examine the diffraction patters of different BTNF concentration and therefore determining the β-phase crystallinity of the structures. Scanning electron microscopy (SEM) was used to capture views of the nanofiber orientation and the surface morphology. The dielectric properties were measured by an impedence/gain-phase analyzer. Results showed that thinner syringe nozzles disturbed the flow of material, resulting in the random alignment of the BTNFs. The best alignment was achieved with a 2.5mm nozzle. In the XRD spectra, peaks consistent with β-phase were more prominent at higher concentration of nanofibers, with a dielectric constant measured at 200 at 1KHz [9].

Electric Polling-Assisted Additive Manufacturing

Electric polling-assisted additive manufacturing or EPAM is a newly developed 3D printing method. By integrating in-situ poling on standard FDM machines, piezoelectric PVDF samples can be directly obtained, without the need of any further post-processing. Researchers of the University of South Carolina, USA describe EPAM as a single design, production and fabrication process. Stock PVDF material in filament form was fed to an FDM machine. The material is molten at a temperature of 230°C and extruded by a 0.4mm nozzle. During the printing, the thread of extruded material undergoes mechanical stretching (Fig. 8). In the meantime, a high electric field was applied between the nozzle and the printing substrate, which act as electrodes. It was observed that too high electric fields might incur burning, due to electrical breakdown, so the maximum investigated field was 2 MV/m. These combined conditions promote the alignment of the dipole moments and thus enable the formation of β-phase crystalline structure. Thin 10cm strands of PVDF samples were printed, with the nozzle tip at a distance of 0.3mm from the substrate. It was found that Kapton tape aided the adhesion of the sample on the printing surface, which was heated to 100°C. Fast Fourier Transform Spectroscopy (FTIR) was utilized to assess the crystalline phase of the specimens. Results showed peaks at 87 cm^{-1}, which is characteristic of the β-phase. Higher poling fields resulted in sharper peaks and also stronger piezoelectric response, with the output current reaching 0.37nA and charge of 4nC, when the devices where mechanically excited. They also produced more complex devices on a flexible substrate and longer PVDF strands, whose output reached 1.5nA and charge of 12nC [31].

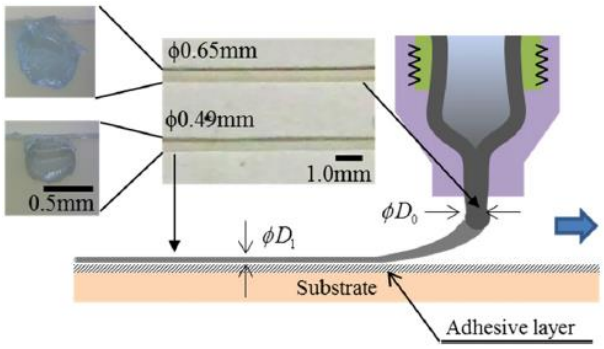

Fig. 8. Visualization of EPAM stretching and poling [31]

In a more recent attempt, a team of researchers expanded on the topic of in-situ EPAM by creating ~0.65mm PVDF films, with integrated 3D printing and corona poling (IPC) (Fig. 9). The difference of this EPAM method is that corona poling is conducted in a second step. After the PVDF layer is printed, the printing tip follows the same path above part and high voltage is applied. To avoid electric breakdown, insulating Kapton tape was used on the substrate, but with the addition of typical paper masking tape, to help with the part adhesion. The specimen was printed as a single layer using a concentric printing pattern. Corona poling voltages up to 13.3 MV/m were applied. The β-phase content of the specimen was detected by FTIR and by observing the infrared spectrum absorption at th 840 and 1279 cm^{-1} bands. For measuring the piezoelectric response, the films were fixed on a fatigue cycling loading frame and segment of copper tape were attached on each end. The output was captured with a picoammeter. The FTIR spectra showed increased that the β-phase content increased to 56.83% at the highest IPC voltage. However, it was noted that the increased heated bed temperature has a negative impact on the crystallinity and it was speculated that higher bed heating causes depolarization. The highest output current of 0.106nA was measured for films poled at 12kV. The d_{31} piezoelectric coefficient was calculated to have an increase of $4.8x10^{-2}$ pC/N. A stress-strain characteristic was also obtained, with IPC PVDF films poles at 12kV having a higher strength (~16.5% increase), but lower strain (6.8% decrease) [3].

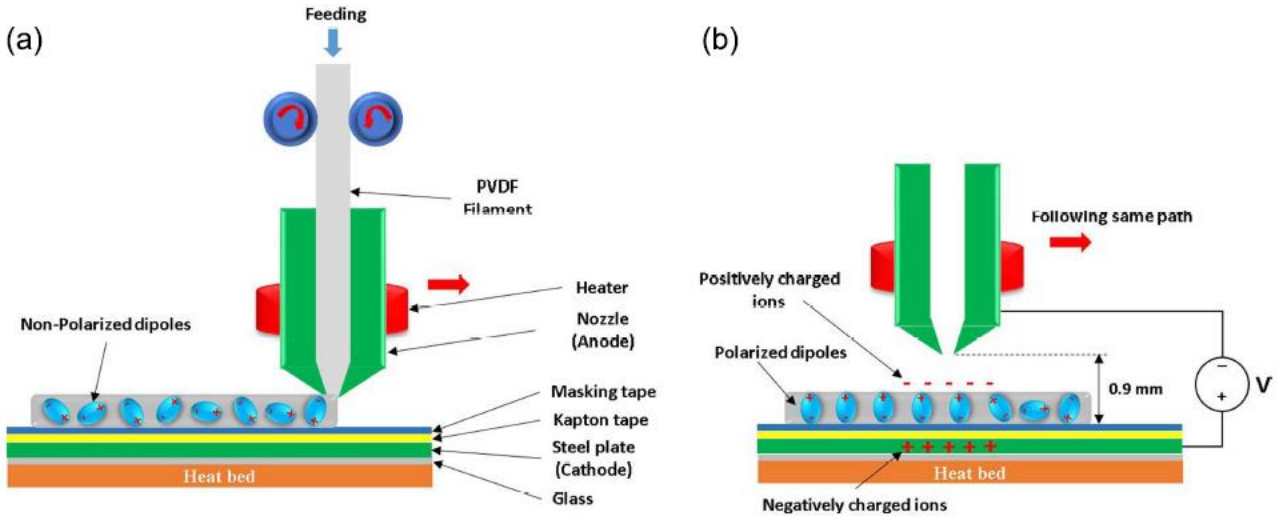

Fig. 9. IPC 3D printing (a) and corona poling (b) [3]

2.3. Fabrication of PVDF-based 3D printing Materials

Solvent Casting Methods

Literature review revealed that there are several methods PVDF and its nanocomposites might be prepared as stock material for 3D printing. In the previous section, liquid inks were introduced. Chen et. al prepared their inks with a solution of DMF and MWCNT or GR at a concentration of 0.03wt%. After the sonication of the solution, PVDF powder was added and an additional sonic agitation step was performed, before transferring the ink to a syringe with a 0.33mm nozzle [30]. Similarly, for BTNF reinforced inks, a set of precursor materials containing barium, titanate and solvents was prepared into a homogenized solution and then loaded into an electrospinning machine, in order to produce the BTNFs. After the fibers were dried, they were introduced in a homogenous solution of 30wt% PVDF in NMP. The content of BTNF was up to 20vol%. The solution was further homogenized by sonication and the resulting paste was transferred to a syringe mounted on a 3D printer [9].

While inks were proven to be a viable option for 3D printing materials, they are more difficult to prepare and process compared to the filament stock material used in other research. Kim et al. have published several papers on the processing of PVDF composite filament in standard FDM machines. The synthesis of these filaments generally followed the same flow (Fig. 10). The process starts with solvent-casting of the base materials, which include PVDF powder and the chosen additive. Their researcher mainly focused on $BaTiO_3$, but they also explored MWCNTs. PVDF powder was dissolved in a DMF solution and the ceramic or carbon nanotube powder was mixed with a magnetic stirrer at high temperature. The solution was ultrasonically agitated. After a homogeneous mixture was achieved, the solution was poured onto a substrate and allowed the DMF to evaporate. That resulted in thin composite sheets. The sheets were then sliced into small segments and fed to a filament extruder machine. The resulting product was a filament of diameters ranging from 2.7 – 2.9 mm [3, 6, 32].

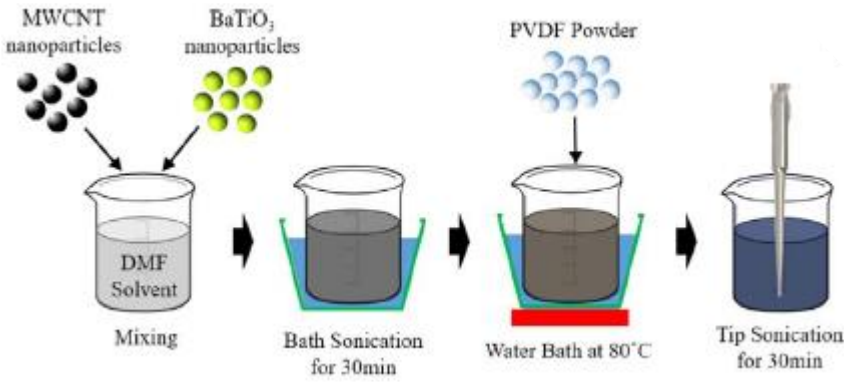

Fig. 10. Solvent casting process of MWNCT/ $BaTiO_3$/PVDF nanocomposite solution for filament extrusion [32]

Melt Extrusion Methods

However, the use of DMF in the aforementioned fabrication techniques poses significant health risks and environmental concerns. In fact, it has been shown that occupational exposure to DMF can lead to liver disease and its hepatotoxicity has been noted [33]. Moreover, the preparation procedure of these 3D printing stock materials is more complex and calls for use of specialized equipment.

Therefore, more straightforward and safe methods are reviewed, which do not use any solvents. Hot melt extrusion for filament fabrication is a common alternative. Kim et al. prepared virgin PVDF 2.7mm filament using PVDF pellets and extruding on a desktop filament extrusion machine at 195°C. They emphasized the importance of preventing contamination during extrusion [3]. Similarly, Kynar 740 pellets were used in a single-screw filament extruder at 210°C, yielding filament of 1.75mm with ±0.15mm tolerance (Fig. 11) [34]. In another study, it was also shown that hot extrusion is also viable for PVDF composites. Farina et al. used a twin-screw extruder to compound PVDF raw material with $BaTiO_3$ and graphene, at concentrations of 78%, 20% and 2% respectively. The materials were processed at 200°C and a filament of 1.75mm with ±0.05mm accuracy was produced [35].

Fig. 11. Raw PVDF pellets and extruded filament [34]

An important consideration for heat molding or extrusion of PVDF is the temperature parameters. The Arkema white paper on injection molding of Kynar® offers useful guidelines on the process conditions. According to the paper, there are two key temperature points. The first point is the actual desired melt temperature, which may vary according to the various PVDF grades and copolymers. The second point is recommended to be at least 17°C above this melting point. In a setup with multiple heating zones, the set temperatures of each zone are "stair stepped" between these two temperature points (Table 1). The exit point of the setup should be set to the appropriate melt temperature. Generally, melt temperatures are reported to be in the range of 200-260°C. Another consideration is the fill speed and pressure. Arkema recommends slow fills speed to prevent the formation of surface defects and rapid pressurization of the material and the gases produced during melting [18].

Table 1. Example of processing temperatures for Kynar® PVDF [18]

Heating zone	**Temperature**
Barrel Zone 1	410°F (210°C)
Barrel Zone 2	420°F (215.6°C)
Barrel Zone 3	430°F (221.1°C)
Barrel Zone 4	440°F (226.7°C)
Nozzle	430°F (221.1°C)

Other significant parameters of the hot extrusion process are outlined by a paper researching the fabrication of polylactic acid (PLA) filaments and their printable performance. Most importantly, the effect of the extrusion temperature and screw speed on the diameter of the filament were investigated. The findings indicate that increased extrusion speed, while the melt temperature was constant, resulted in increased filament diameter, due to swelling of the melt volume when exiting the

extruder's die. Furthermore, the relationship of diameter and extrusion temperature was shown to be inverse. This was attributed to the reduced viscosity of the polymer and therefore the improved flowability, which stretched the filament thinner than the die's diameter. The paper also mentions that there is an optimal extrusion speed and temperature setting which leads to the best tensile strength of the produced filament [36].

Regarding the filament's diameter, two sizes are widely available for the most common FDM machines: 1.75mm and 2.85mm. By observing the various filament suppliers, it is made evident that 1.75mm filament is more prominent, even in the case of specialty materials like PVDF [37, 38]. Also, an added benefit of 1.75mm over the other standard diameters is that it is easier to process. The 3D printer heater block can melt this filament faster and the force required by the extruder is less, due to the lower pressure within the nozzle. Also, the control of the extrusion rate can be finer, because per unit of filament length, the extruder pushes less material through the system [39].

2.4. FDM Printing Parameters

This section aims to collect all the information related to FDM printing parameters which proved to work well for processing PVDF and PVDF-based filaments. Scientific papers explore these parameters in various degrees of detail, with the main focus being on general conditions and 3D printer type, temperature settings, printing speed, layer and shell thickness, infill pattern and percentage.

Experimental work for EPAM process showed that an increased nozzle temperature of 230-250°C and bed temperature of 90-100°C promoted the flowability of PVDF filament, prevented cooling induced warping and improved bed adhesion [3, 10]. However, another source reported potential thermal degradation at nozzle temperature higher than 230°C. Also, it has been reported that printing at temperature >230°C might cause the accumulation of material around the printing nozzle and may cause the release of dangerous gases (Fig. 12) [10]. Emphasis was given on the positive effect of increased temperature on the neck growth and adhesion to neighboring printed structures. They also confirmed that a build platform heated at 105°C helped with yielding dimensionally accurate parts [34].

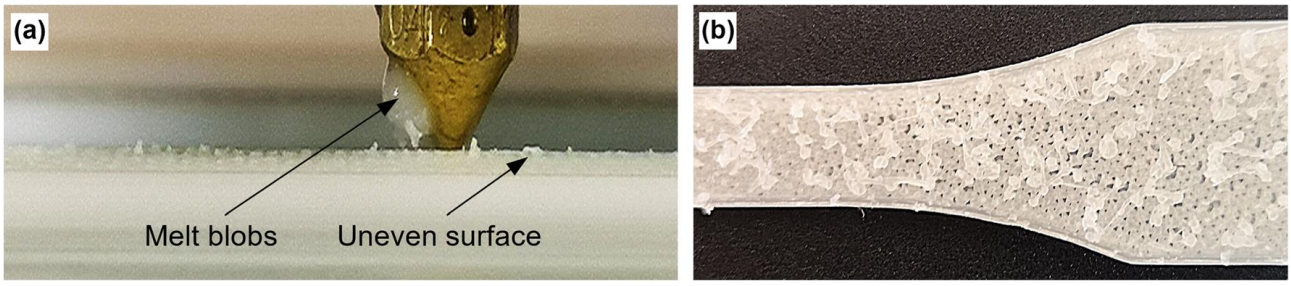

Fig. 12. Extrusion temperature related artifacts.
Blobs due to high temperature (a) and underextrusion due to low temperature (b) [10]

An extruder feedrate of 200 mm/min (33.3 mm/s) and filament feedrate of 30 mm/min (5 mm/s) were reported to be successful at fabricating thin PVDF samples [31]. Thin films were also fabricated at low speeds of 10 mm/s [3]. While higher printing speed accelerates the process, it has been noted that lower speed in the 10-25 mm/s range prevent rapid cooling and assist interlayer bonding. Higher speeds resulted in poor surface finish and layer bonding [34]. Similar findings are shared by other

papers, which mention that processing at low speeds of around 20 mm/s is more likely to result in a successful print [10].

The effect of different infill parameters was investigated by Mullaveettil et al. Different patterns were tested from the selections found in the Ultimaker Cura slicing software. Infill percentage was kept constant at 75%. Under bending, the infill patterns was reported to not have a big influence. However, it was shown that the concentric printing pattern, while increasing the possibility of part distortion, is the one which yields products of superior mechanical characteristics, with tensile strength of 32.3MPa, and high ductility [40]. The tensile strength has also been shown to be proportional to the infill density, with parts filled at 100% having the best strength characteristic [10].

Other considerations for printing conditions are also detailed. Build plate adhesion has been noted as a critical concern. Bed adhesion aids included Kapton tape, smooth or rough glass, copper sheet, adhesive tape (commonly referred to as "painter's tape") and special 3D printing adhesives. Among these options, simple adhesive tape and Dimafix ® special adhesive lead to good adhesion. Additional provisions included the addition of extra perimeter lines on the first printed layer (also known as brim), in an effort to increase the surface contact area between the part and the build platform [31, 40].

2.5. Testing Methods

PVDF and PVDF composite specimens can be tested both for their mechanical and piezoelectric properties. For this purpose, a variety of testing methods might be utilized.

For the investigation of the piezoelectric properties, researchers are interested in evaluating the β-phase crystallinity of PVDF after it has been poled or reinforced with additives. A widely used technique is the Fourier Transform Infrared Spectroscopy or FTIR. The spectra generated reveal absorbance peaks at certain wavenumbers, with 840, 874 and 1279 cm^{-1} being characteristic of the β-phase crystalline structure. The α-phase content can also be estimated using this technique, so the percentage of β-phase over α-phase content can be determined [3, 31, 34]. An alternative technique to examine the β-phase crystallinity is X-ray diffraction (XRD). The reflection plane that corresponds to the β-phase is the (110) plane. Fig. 13 shows an example of FTIR absorbance spectra of an EPAM fabricated sample. A peak at 874 cm^{-1} is evident at 874 cm^{-1}, which becomes more prominent as the poling voltage increased [34]. The dielectric constant and piezoelectric coefficient can be measured with specialized instruments (e.g d_{33} meter) or they can be mathematically derived, by measuring the current output of the device [41].

For the investigation of the external and internal sample morphology, scanning electron microscopy (SEM) was often employed. The technique was used to review imperfections (e.g. microporosities, cracks or agglomerates) and dispersion of particles in the PVDF matrix [9, 30, 34]. Examples of SEM captures are presented in Fig. 14. Surface roughness was also evaluated with this technique [35].

For the mechanical characterization of 3D printed samples, a Dogbone specimen was often used to determine the tensile strength. In the case of thin films, no standard tensile strength specimens were used, but stress-strain curves could be derived (Fig. 15). Reported figures for tensile strength were in the range of 30-40 MPa [3, 34, 35, 40].

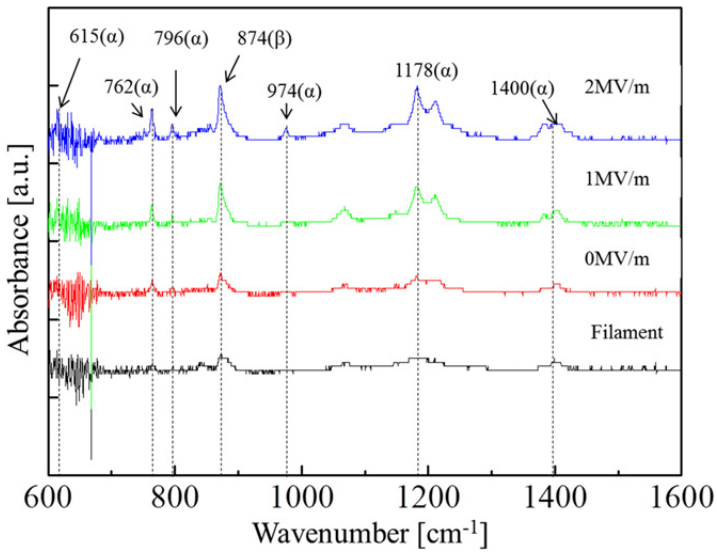

Fig. 13. FTIR spectra of specimens poled at different electric field intensities [34]

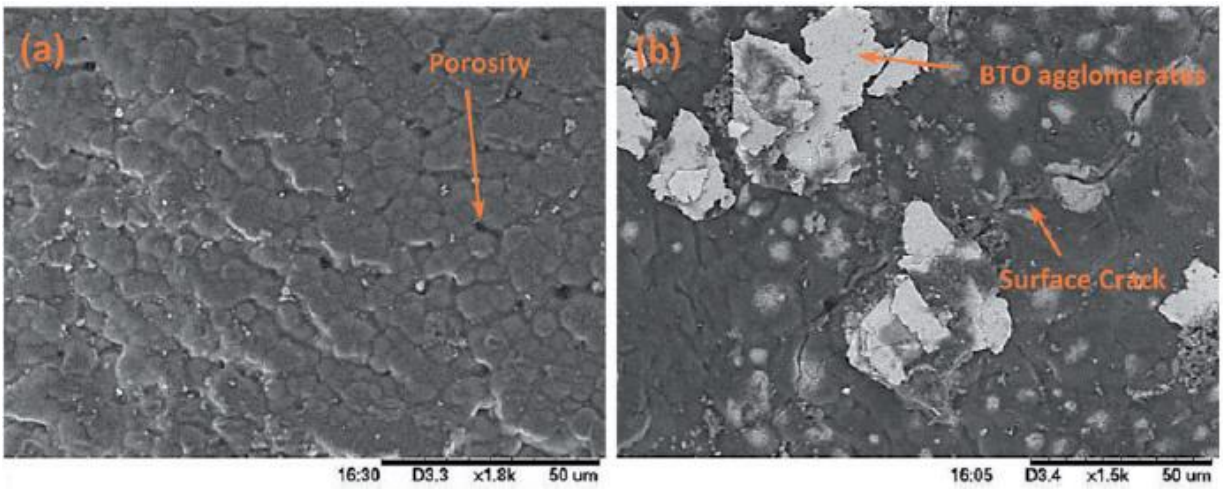

Fig. 14 SEM images of PVDF/ $BaTiO_3$ films fabricated via solvent casting (a) and 3D printing (b) [41]

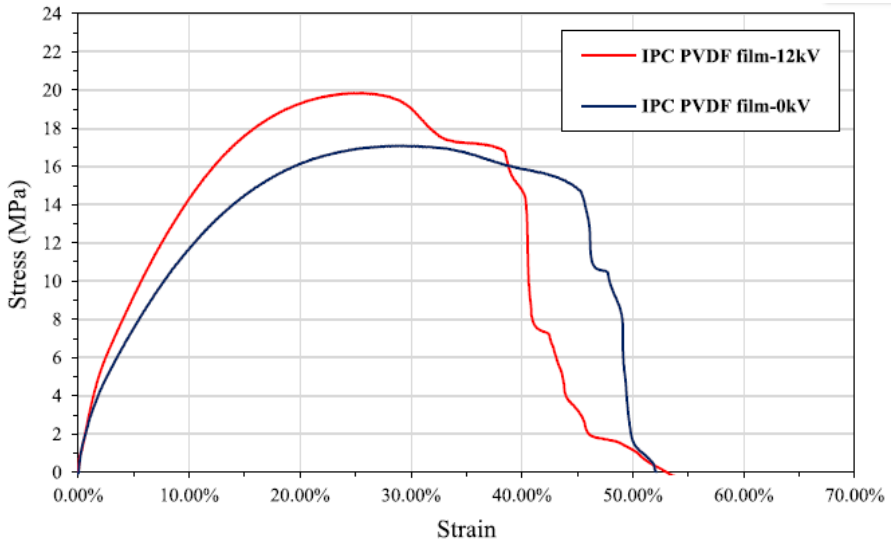

Fig. 15. Stress-strain curve of IPC fabricated PVDF films [3]

2.6. Conclusions

The literature review revealed the importance of the PVDF and PVDF-based nanocomposites, especially in the case of additively manufactured structures used in energy harvesting and sensor applications. The PVDF β-phase crystalline structure was highlighted as the most relevant, due to the intense piezoelectric behaviour it exhibits. Methods of enhancing the piezoelectricity of PVDF were investigated and they included poling and doping with various types of fillers. Ceramic fillers like $BaTiO_3$, have been reported to significantly improve the β-phase content of the PVDF nanocomposite. Fabrication of PVDF films was achieved via methods like spin-coating or the Langmuir–Blodgett process. 3D printing material based on PVDF might be prepared in liquid ink form and processed with a technique known as Direct Ink casting. Also, PVDF filaments can be produced into filament form for FDM printing. Common techniques included the preparation of PVDF suspensions in liquid solvents and the addition of additives like $BaTiO_3$ or MWCNTs. After the evaporation of the solvent, the thin sheets of nanocomposite were segmented and hot extruded in a filament extruder machine. Another viable technique was simple compounding of the PVDF and its additive materials and direct hot extrusion. The β-phase content of PVDF samples was evaluated using methods like FTIR and XRD. Piezoelectric parameters were tested with precision instruments like picoammeters or d_{33} meters. SEM was used to investigate the morphology of the samples, while tensile strength testing was used to mechanically characterize the parts.

3. Methodology

This chapter presents the methodology of the experimental work in detail and it is organized in two parts: filament extrusion methodology and FDM 3D printing methodology. The methodological procedure for each part is presented in the process flow diagrams of Fig. 16 and Fig. 17.

Filament extrusion

The first step of the process is the equipment selection; particularly the type of hot melt extruder and the accompanying accessories (i.e. devices for cooling, pulling and winding the filament). At this stage, the default control electronics and mechanical subassemblies are evaluated and necessary alteration can be made as required. Then, the extruder's heating zones parameters are selected and the system is allowed to preheat at the set temperatures. The feedstock material composition and form are selected. At the beginning of the experimentation, a low-cost material in pellet form is used (polylactic acid), in order to familiarize with the system and roughly determine what parameters works well with processing thermoplastics. In a later stage, the feedstock is replaced with the materials under investigation (i.e. PVDF and mix of PVDF / $BaTiO_3$). Regarding the material form, it might be either in its original form, repurposed material from previous experimentation or a mix of the two. After the material is loaded, the extrusion screw is activated at a constant speed, which is experimentally determined. Once a sufficient length of product is extruded, the screw is deactivated and the filament is routed through the pulling mechanism. Afterwards, both the screw and puller are activated the chosen speeds. The end of the filament is directed to a spool where it is collected. Finally, the cooling device is activated and continuous extrusion is initiated. The dimensional accuracy of the produced filament is evaluated in real-time using a thickness gauge dial and parameters are adjusted as needed. If it is observed that the dimensional deviation is unacceptable (greater than ±0.1mm from the target diameter), the segment of filament is cut and the process parameters are reconsidered, therefore allowing for an iterative process of determining the optimal system parameters and controlled variables. The rejected filament is then converted to pellet form once again and it can be reintroduced in the system. Once a length of filament of acceptable dimensions is obtained, it is collected for later use in an FMD 3D printer. All information regarding the selected system parameters and detailed procedure are presented in section 3.1.

FDM 3D printing

3D printing is also an iterative optimization process, which begins by selecting the specific 3D printer system. A test specimen is chosen based on the kind of testing that the fabricated sample might be subjected to. The specimen's 3D model is then loaded on the Slicing software of choice, the Slicing parameters are configured and machine code (G-code) is generated. The code is transferred on removable storage drive, loaded on the 3D printer and the printing process is initiated. The entire printing of the first layer is closely monitored, so to promptly detect any extrusion or adhesion issues. If the first layer is unproblematic, the procedure is allowed to continue; otherwise, the printing is interrupted and the Slicing parameters are reevaluated. The printing of the subsequent layers is periodically checked to detect clogging or under-extrusion problems. Again, if any such defects are observed, the printing is interrupted and the Slicer settings are changed. Once a full specimen is successfully obtained, it is allowed to cool and its surface morphology is visually inspected for any defects. In the end, if the specimen is deemed acceptable, it is collected for later testing and the system parameters are recorded. All information regarding the selected system parameters and detailed procedure are presented in section 3.2.

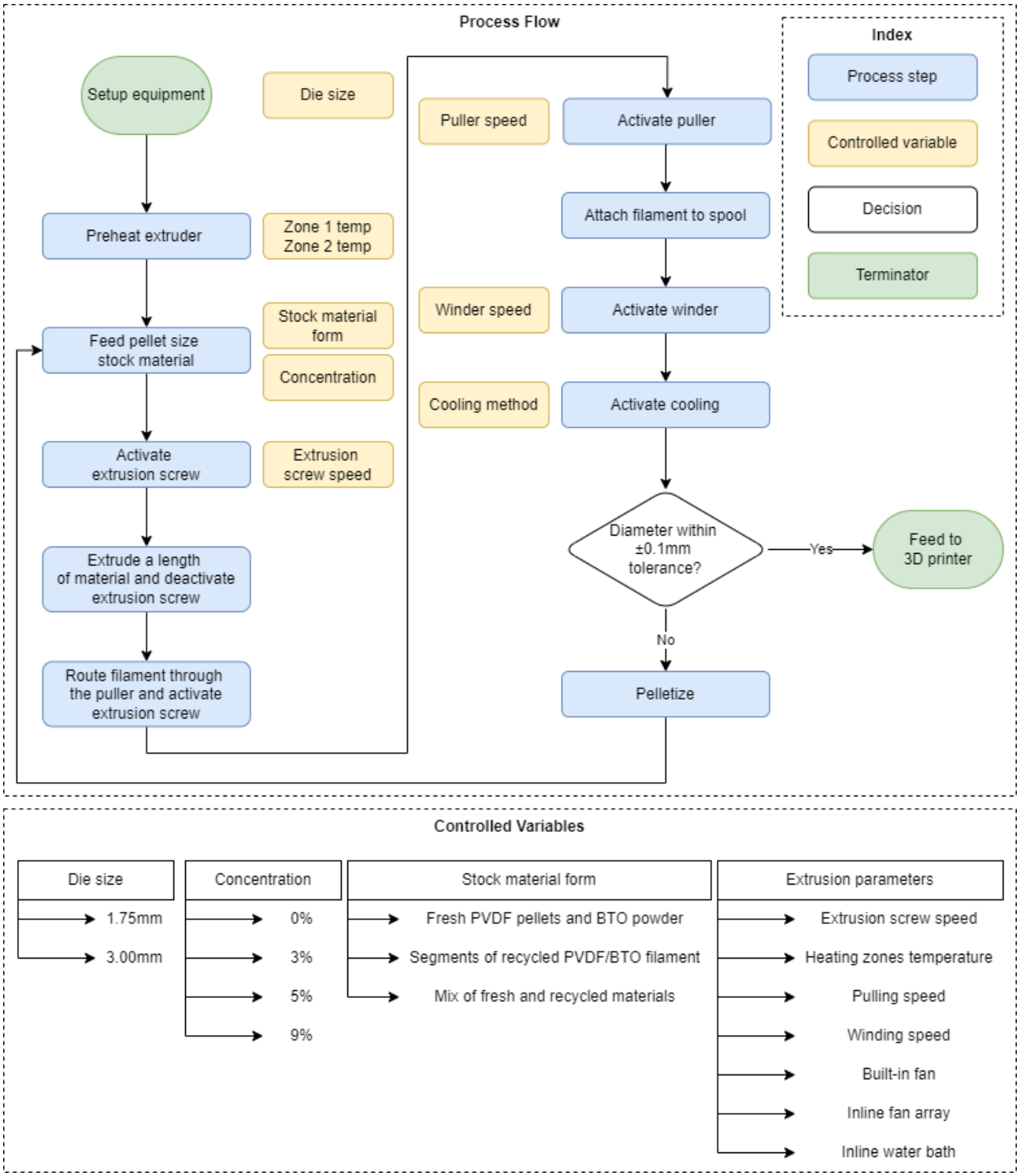

Fig. 16. Flow and controlled variables of filament extrusion process

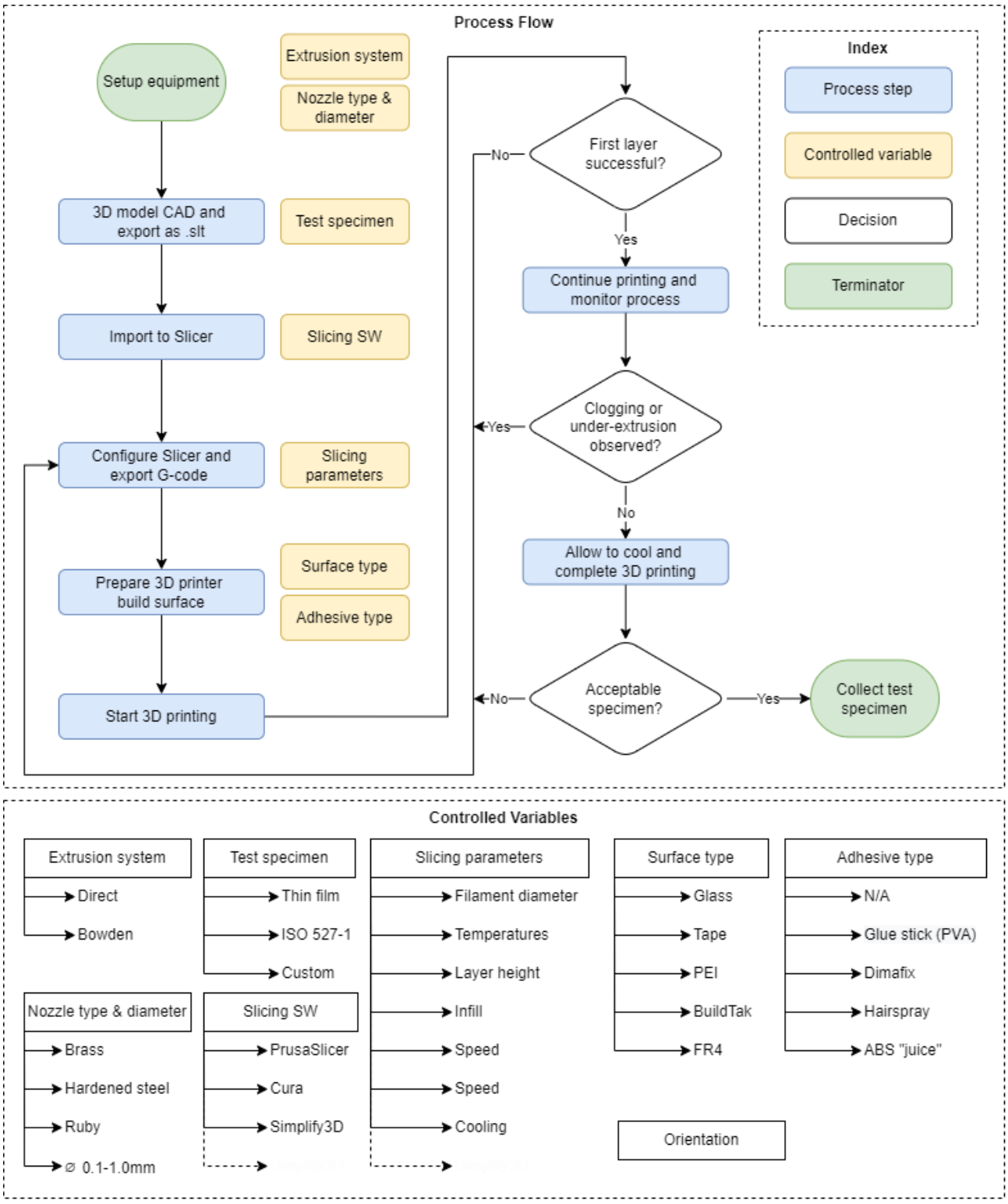

Fig. 17. Flow and controlled variables of filament 3D printing process

3.1. Filament Extrusion

The first part of the experimental procedure aims to produce the PVDF filament with certain concentration of $BaTiO_3$ inclusions. The main consideration is to optimize an existing hot filament extrusion system to process pellet size polymer stock material and ideally yield a perfectly circular filament of 1.75mm diameter, compatible with the most common FDM 3D printing systems. Due to the high cost of the PVDF and $BaTiO_3$ components, the experimentation starts with more affordable polylactic acid (PLA) pellets. Having determined the system parameters and variables that work best for achieving a consistent PLA filament, similar principals are applied in order to create the PVDF/ $BaTiO_3$ composite filament. The geometric consistency of the material can be accessed in real time using a dial thickness gauge and after the process using calipers. The process capability is determined by checking the dimensional tolerance and using statistical indices. If the quality is deemed acceptable, the filament is then used for 3D printing. If the dimensions are not within the defined tolerance, the filament is cut to pellet size and repurposed, therefore minimizing the waste material produced.

In this section, the used materials, the experimental setup, parameters and experimental procedure of the filament extrusion system are presented. The final setup is determined through an iterative process of trying different equipment configurations and adjusting the system's variables.

3.1.1. Materials

The materials used for the experimental work included PLA pellets provided by Formfutura, PVDF pellets provided by Sigma Aldrich and $BaTiO_3$ powder provided by Inframat Advanced materials.

PLA

PLA pellets of clear colour and cylindrical shape were acquired from Formfutura. The pellet diameter is 2.85mm and their length is approximately 5mm. The main properties according to the pellets' technical datasheet are given in Table 2.

PVDF

The used PVDF raw material comes in pellets of size 5.65mm in diameter and 1.45mm in height. The product is acquired from Sigma-Aldrich and has a product code SKU 427160-100G and it cost 57.9€ per 100gr. Table 3 presents the material properties as specified by the supplier.

$BaTiO_3$

$BaTiO_3$ is purchased from Inframat Advanced Materials in powder of particles sized 500nm in average. Its product code is 5622-ON5 and it is priced at ~50€ per 250gr (with cost decreasing if purchased in larger quantity). The main material properties are presented in Table 4.

Table 2. Formfutura PLA pellets specifications [42]

Property	**Specification**
Specific gravity	1.24 g/cc
Melt flow rate	6.00 g/10min
Impact strength	7.5 KJ/m^2

Property	Specification
Tensile strength	110 MPa
Tensile modulus	3310 MPa
Elongation at break	160%
Flexural modulus	± 55.2 MPa
Hardness	± 2392.5 MPa
Print temperature	± 180-220 °C
Melting temperature	± 210±10 °C
Viscat softening temperature	± 60 °C

Table 3. Sigma-Aldrich PVDF pellets specifications [43]

Property	Specification
Quality level	100
Form	Pellets
Melt index	3.5-7.5 g/10 min (230°C/12.5kg)
Mol wt	average Mn ~130,000 average Mw ~400,000
Impact strength	12-20 ft-lb/in. (Izod, ASTM D 256, notched)
Dielectric constant	9.4-10.6, 100 Hz (ASTM D 150)
Hardness	65-70 (Shore D, ASTM D 2240)
Refractive index	n20/D 1.41
Viscosity	23,000-27,000 poise(230 °C) (100 sec^{-1}; typical)(lit.)
Transition temperature	brittleness temperature -62 °C (ASTM 2800) Tm 140-145 °C (ASTM D 3418)
Density	1.77 g/mL at 25 °C

Table 4. Inframat Advanced Materials $BaTiO_3$ powder specifications

Property	Specification
Purity	99.95%
Particle size	500nm avg.
Melting point	1620°C
Density	5.85 g/cm3

3.1.2. Equipment Selection and Description

The procedure starts with the selection of the equipment. Two systems are initially considered from two different manufacturers: Noztek (Noztek Touch) and Wellzoom (Wellzoom Desktop Extruder Line) (Fig. 18). While the Noztek is a standalone extruder, the Wellzoom system also comes with puller and winder mechanisms. Both of the systems are tested using PLA pellets to access their performance. Their operation is analyzed by studying the manufacturer's documentation and by reverse-engineering their main control systems.

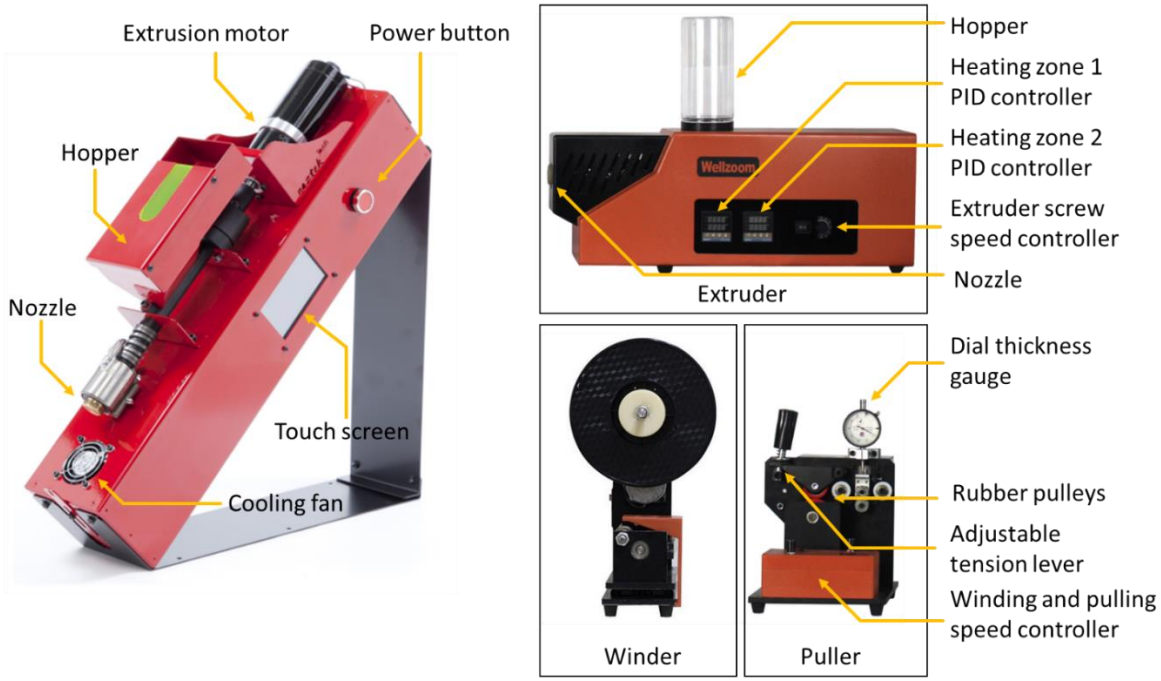

Fig. 18. Noztek Touch extruder (left) [44] and Wellzoom Desktop Extruder Line (right) [45]

The selection criteria are ease-of-use, controllability of the process parameters, cleaning possibility and overall stability of the system. For the purposes of producing a high-quality nanocomposite filament, fine and precise control over the process parameters is deemed critical. It should be possible to adjust the extrusion speed, heating zones temperature in real-time and have a system with low inertia and quick response to these changes. Also, feedback on the precise values of these parameters is preferable. Regarding the cleaning possibility, this is another important consideration. If there is a need to change over to a different material or material concentration, the system should be able to be cleaned to a satisfactory degree, so there would be no cross-contamination between the different samples. This way, the mixing of old and new material can be minimized, which in turn results in minimized waste material. This is feature is particularly relevant for this experimental work, due to the high cost of the raw materials.

Wellzoom Extruder

The Wellzoom extruder features two heating zones, each individually controlled by a PID controller. The temperature can be set on these controllers and the target and real temperature values are shown on the displays. The extrusion screw speed is also controllable via an analogue knob. The knob is marked in increments of 10 units, from 0-90, but it is not specified what these units corelate to. Upon power up, the machine automatically turns on both heating zones. The heating elements remain activated until the target temperatures are reached. However, in reality it is observed that the PID control parameters are poorly configured. At a set target temperature of 200°C, the actual temperature quickly rose and overshot the target by 30-40°C. This is undesirable, because the residual material within the screw overheats and there is an increased risk of degradation of the polymer and carbonization of particles. Furthermore, the heaters and extruder are all wrapped in insulation and additional parts are bolted and attached in one assembly, making it impractical to disassemble and thoroughly clean the machine. For these reasons, the Wellzoom extruder is not the best option for conducting the experimental work.

Noztek Extruder

On the other hand, the Noztek extruder features a touch screen interface, which allows the user to control various parameters with sufficiently fine precision in straightforward manner. The two heating zone temperatures, extrusion speed and cooling fan can be controlled from the screen interface. The units of each parameter are displayed on the screen, providing real-time feedback of the process. These parameters are the set and actual temperatures of the heating zones and the set and actual speed of the extruder motor, which includes a built-in encoder. The PID control is also better, with the temperatures steadily rising to the target values and not exceeding them. The nozzle is easily exchangeable and any residual material can be pulled out from the extrusion tube, while heating it a low temperature, allowing for good cleanup of the system, in preparation for a different material composition. Therefore, the Noztek extruder is the best candidate for this work and it is part of the final equipment configuration.

Puller and Winder

Previous experimental work has shown that freely extruding the filament and allowing it freely flow under its own weight does not yield a high-quality product, with the diameter fluctuating greatly (±0.2mm) and roundness being inconsistent. In an effort to more closely control the process, the additional components of a puller and winder are introduced.

The Wellzoom Desktop Extruder Line is delivered with these components. The puller consists of a simple rubber pulley (⌀48mm) assembly which is driven by a stepper motor. A toothed 8mm GT2 pulley is fixed on the output shaft of the motor. The motor pulley is coupled to the rubber via a timing belt loop. This results in a reduction ratio of 1:6, therefore increasing the pulling torque. The filament is fed to the puller through a pair of bearings; one is stationary and the other is mounted on base that is free to move in the vertical direction. Upon the base rests the tip of an analogue dial thickness gauge. This setup allows to monitor the diameter of the filament produced and quickly evaluate if the system parameters need adjustment. This real-time measurement is more preferable over measuring the diameter after a sample has been produced. In the latter case, if the sample is measured exceed the tolerance, then it would have to be discarded. In the former case, this waste can be minimized, by quickly correcting the extrusion variables “on the fly”. The puller’s tension is also adjustable via a spring-loaded lever. The control electronics for the puller and winder motor are also found on this assembly.

The winder mechanism is designed to hold an empty spool where the filament is coiled. It is driven by two motors. One motor is continuously working at a fixed speed and it control the linear movement of the spool along its central axis. This motion ensures that the filament is evenly distributed across the spool and throughout its entire length. The second motor (hereinafter winding motor) drives the rotational movement of the spool. Its speed is adjustable from the controls found near the puller mechanism.

Pelletizer

An additional piece of equipment is designed and prototyped, whose purpose is pelletize filament. It consists of a 3D printed body which house a Forstner bit meant for wood drilling. A hexagonal M4 threaded insert is placed close to the cutting edges of the bit. The filament is manually fed through

the insert and the bit is driven by a handheld drill. A bearing is fitted on the lid of the device to support the free end of the bit.

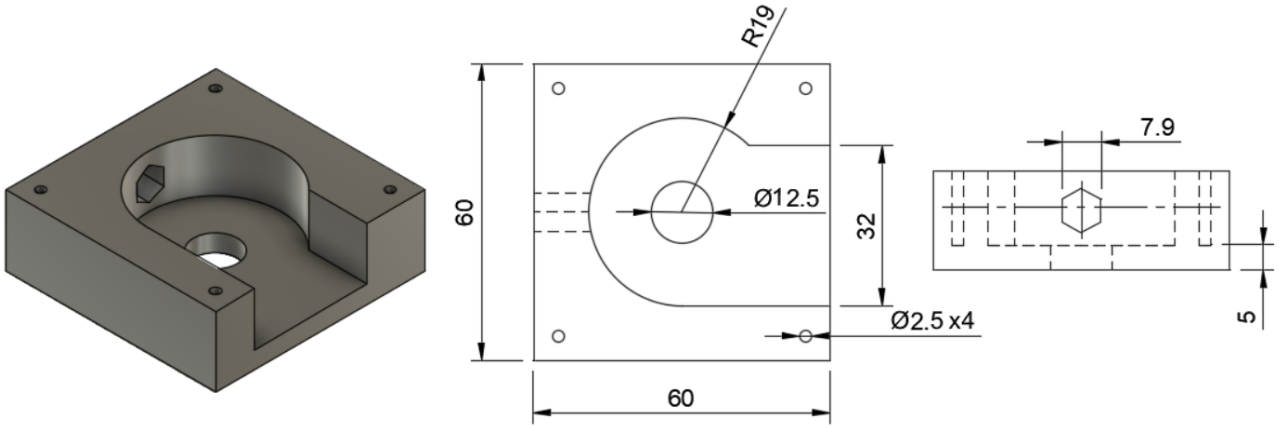

Fig. 19. Original prototype of filament pelletizer

Control Electronics

As mentioned above, the puller and winder share the electronic controls. These mainly consist of the activation switches, the speed control potentiometers and stepper motor driver circuits. It is deemed important to further analyze and understand the working principals of these electronics. While they offer a good degree of controllability, the goal is to be able to know exactly the variables of the system and have fine control over them. The operation of the two switches is straightforward; they enable or disable the puller and winding motor individually. The potentiometers are used to adjust the speed of each motor. The most complicated part is the stepper motor driver circuits. They are built around the Allegro A4988 bipolar stepper motor driver integrated circuit (IC). The IC is already mounted on a printed circuit board (PCB), along with the necessary peripheral electronic components. For the scope of this work, the focus is mostly on the control signals required by the A4988 board.

The DIR and STEP signals are mainly responsible for the motor control. The logic state of the DIR pin determines the direction of rotation. The STEP input expects logic high pulses. For each received pulse, the controller drives the motor one microstep. The microstepping resolution is determined by the MS1, MS2 and MS3 signals according to Fig. 20 [46].

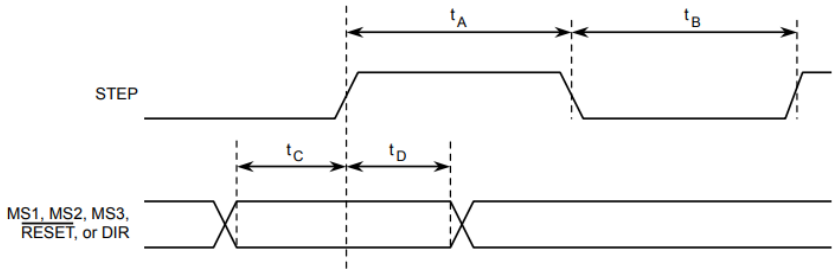

Time Duration	Symbol	Typ.	Unit
STEP minimum, HIGH pulse width	t_A	1	µs
STEP minimum, LOW pulse width	t_B	1	µs
Setup time, input change to STEP	t_C	200	ns
Hold time, input change to STEP	t_D	200	ns

Fig. 20. A4988 control signal timing diagram [46]

In this case, all those inputs are pulled low, so a full step microstepping is selected. Therefore, one STEP pulse equals one step rotation of the motor. With the stepper motor resolution known, we can derive the angular displacement of the motor axis, when it is rotated by one step, also known as step angle. The formula below describes the relationship between resolution and step angle:

$$a = \frac{360°}{n} \tag{3.1}$$

where: a: step angle (°)
n: resolution or number of steps per full rotation

For the common NEMA 17 stepper motor used in the puller mechanism, the resolution is 200 steps per full revolution, therefore the step angle is equal to 1.8°. The motor speed is controlled by the frequency of the STEP pulses. According to the A4988 datasheet (Fig. 20), the HIGH pulse duration must be at least 1μs, followed by a LOW pulse of minimum equal duration. Therefore, the STEP signal frequency cannot have a period less than 2μs or frequency higher than 500kHz. The relationship between STEP frequency and rotational speed can be calculated as follows:

$$RPM = \frac{a}{360°} \cdot f_{STEP} \cdot 60 \tag{3.2}$$

where: RPM: revolutions per minute
a: step angle (°)
f_{STEP}: frequency of STEP signal (Hz)

The STEP signal in the Wellzoom controller is generated by an oscillator circuit, which outputs a rectangular waveform of variable frequency. The oscillator circuit comprises of a 555 timer IC in astable mode (Fig. 21). A 555 astable multivibrator circuit requires only a few external components and the characteristics of its output signal are determined by a set of resistors and a capacitor. The output (pin 3) is periodic and stays at a high level for a time period t_1, also referred to as charge time. t_2 is the time the output is low and it is called discharge time. The timing parameters of the output signal as given in the technical datasheet are calculated as follows [47]:

$$t_1 = 0.693 \cdot (R_A + R_B) \cdot C \tag{3.3}$$

$$t_2 = 0.693 \cdot R_B \cdot C \tag{3.4}$$

$$T = t_1 + t_2 = 0.693 \cdot (R_A + 2 \cdot R_B) \cdot C \tag{3.5}$$

$$f = \frac{1}{T} = \frac{1.44}{(R_A + 2 \cdot R_B) \cdot C} \tag{3.6}$$

$$DC\% = \frac{t_1}{t_1 + t_2} \cdot 100 = \frac{R_B}{R_A + R_B} \cdot 100 \tag{3.7}$$

where: t_1: charge time (output high) (s)
t_2: charge time (output high) (s)
T: period (s)
f: frequency (Hz)
$DC\%$: duty cycle (%)

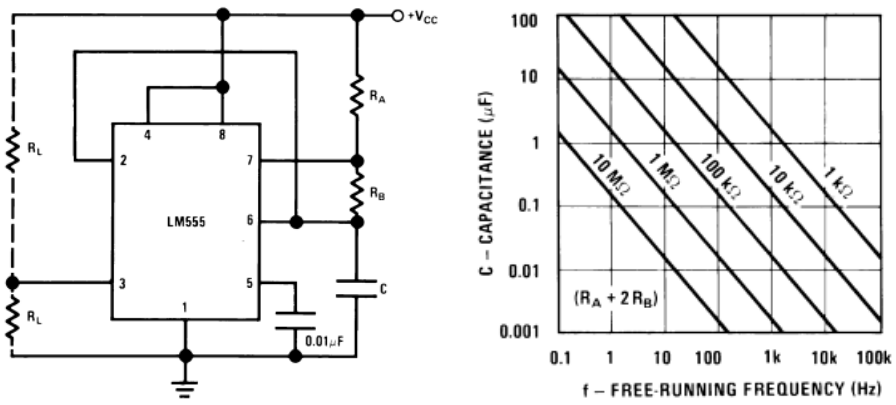

Fig. 21. 555 astable oscillator circuit diagram (left) and RC selection graph (right) [47]

By observing the Wellzoom controller PCB, it is determined that the values for the resistors and capacitor are R_A=3.3kΩ, R_B=0-22kΩ and C=470nF. R_B is the variable resistance potentiometer found on the control box of the puller. By varying the resistance, the frequency of the oscillator's signal can be changed. By replacing the values in formula 3.6, it is calculated that the minimum output frequency is 64.8Hz, while the maximum frequency is 928.4Hz. Then, considering the formula 3.2, the minimum and maximum rotational speed of the motor are calculated to be 19.44 RPM and 278.52 RPM respectively. Taking into account the reduction ratio of the pulley, the puller speed ranges from 3.24RPM to 46.42RPM. Assuming that the filament does not slip, the linear speed at which it is pulled is approximately 0.008-0.122 m/s.

The original controller with the A4988 drivers has certain disadvantages. The A4988 output signal is subdivided in 16 discreet levels which approximates a sinusoidal waveform [46]. This is a low resolution which manifests as audible noise and abrupt stepping of the motor. In turn, this abrupt behavior can be transferred to the filament pulling mechanism, resulting in inconsistent extrusion and imprecise dimensions. Furthermore, it reduces the amount of control the user has over the process. Therefore, the need for a better stepper driver is made evident. A popular one-to-one replacement is the Trinamic TMC2208 IC. The IC also comes mounted on a PCB, which is pin-compatible with the A4988 board (Fig. 22). The TMC2208 implements an efficient motor chopper algorithm (StealthChop2™), which ensures silent and smooth operation, via a 256μStep sequencer. By directly replacing the A4988 with a TMC2208 driver, an immediate improvement is obvious, with the pulley running more smoothly and barely noticeable noise. Consequently, these drivers are selected to be used in the final equipment configuration.

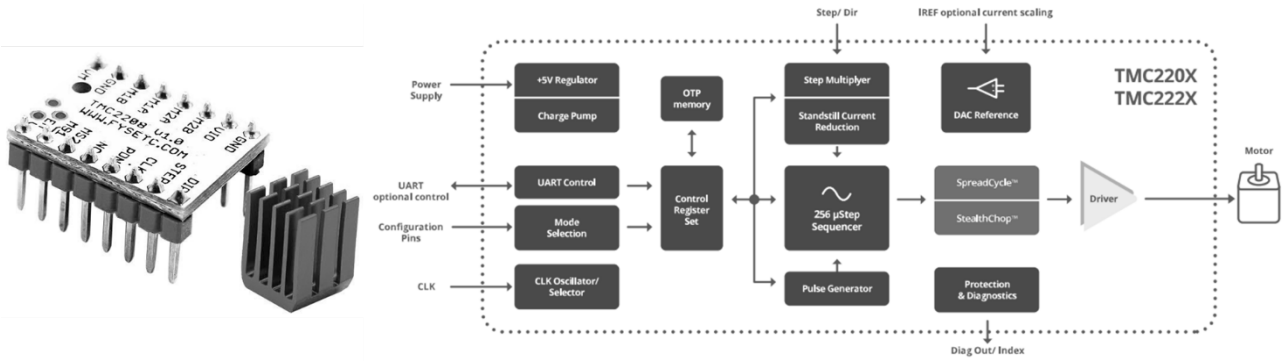

Fig. 22. TMC2208 driver board (left) and functional block diagram (right) [48]

The last consideration for the control electronics is the user input and feedback. For the extruder itself, a sufficient level of control and feedback is offered, via the touch screen interface. On the other hand, the puller and winder controls are analogue and no feedback is available on the precise values of the system parameters. As discussed, the motor drivers need rectangular waveforms to operate, originally generated by the 555 IC. To achieve better control, the 555 IC is replaced by an Arduino microcontroller board. This way, the duration of signal pulses can be precisely configured in software. Analogue controls can also be implemented, by processing the input of a potentiometer and displaying the variable values on the computer or an external display. Two control programs are developed: one with digital control from the computer and one with analogue control from a potentiometer. The control variables are the pulling speed and the winding speed. The output frequency range 50-1000Hz, which, after applying formulas 3.2 and considering the reduction ratio and pulley diameter, translate to rotational speed of 2.5-50RPM and linear pulling speed of 0.007-0.131m/s. For full diagrams and code refer to Appendix 1.

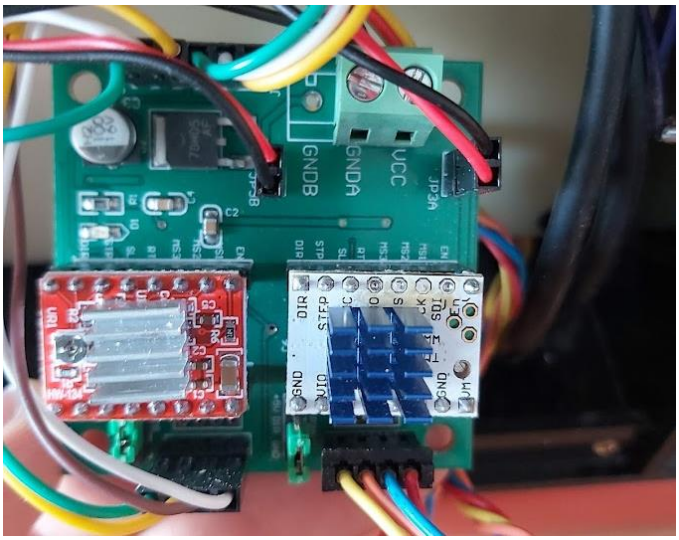

Fig. 23. Original A4988 driver (left) and upgraded TMC2208 version (right)

3.1.3. Experimental procedure

Having determined the experimental equipment, the next step is to develop the procedure itself. Fig. 24 depicts the final filament extrusion setup, while Fig. 16 summarizes the process steps and the various controlled parameters.

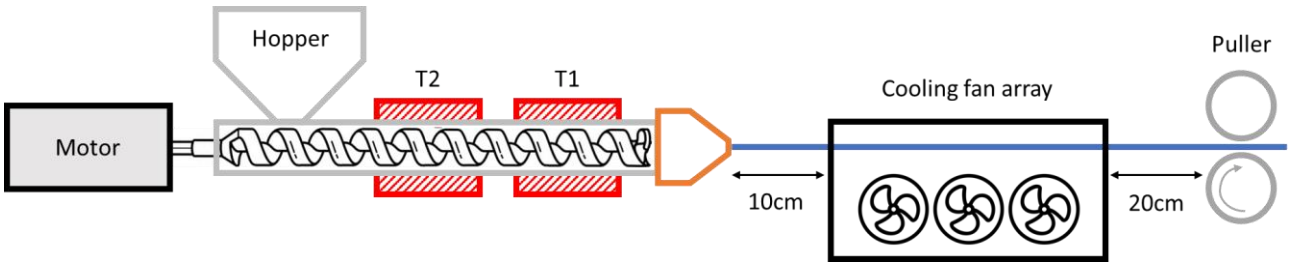

Fig. 24. Schematic of filament extruder system

First, the desired die size is selected and installed on the extruder. The preheating phase of the two heating zones follows. The recommended preheating time is 15 minutes [44]. The set temperatures depend on the stock material used. Then the material is loaded in the extruder's hopper. The form and

composition of the material are determined beforehand. The Noztek extruder is capable of processing polymers in pellet and powder form. Also, the stock material can be either fresh or recycled from low quality lengths of filament previously produced. The composition of the material is relevant for the later steps of the experiments and it refers to the concentration of $BaTiO_3$ particles in the PVDF matrix. This concentration range is selected between 0-9%. The extrusion screw motor can then be turned on. The speed of the screw is another controlled variable. It is configured via the touch screen and the display units are RPM. After a few minutes, the molten material starts extruding through the brass die on the extruder's nozzle. A length of filament is extruded and the screw is turned off, so that the end of the filament can be secured on the puller mechanism. The screw and puller can now be activated. The end of the filament is secured to the spool and the winder is activated. The winding speed is selected so that there would be no tension between the puller and the winder. Finally, the cooling method is selected. There are three options: built-in fan on extruder, inline fan array or inline water bath.

During the extrusion, the filament's diameter is monitored using the dial thickness gauge. It is zeroed out before the beginning of the process, using a calibration rod of 1.75mm diameter. Ideally, the dial needs to be stable and point to the 0 indication. If extreme fluctuations are observed or if the measurement is far from the target, that section of filament is marked. There are two possibilities for the low-quality product; either discard it as waste or cut it back to pellet size and recycle it through the extruder once again. If it is of acceptable geometry, it is kept for further processing in the second step of the experimental work.

3.2. FDM 3D Printing

After a continuous length of filament with acceptable dimensional parameters is successfully fabricated, it is used as stock material for the FDM 3D printing process. The goal is to achieve stable flow of filament through the printer system and attain a full 3D printed specimen for mechanical testing purposes. For this reason, a set of critical parameters which affect the printing quality and bring the likelihood of nozzle clogging to the minimum are outlined. The printing quality is accessed progressively using small specimens and observing the behavior of the 3D printer and the visual appearance of the specimens.

The equipment is selected from a set of commercially available 3D printers. The selection criteria are based on the filament specifications and the findings of previous experimental work. Another critical set of parameters is the settings configured in the Slicing software. Therefore, a program with high degree of customizability of these parameters shall be favored. Ultimately, the target is to observe the printer's performance and obtain a few test specimens to study their appearance and mechanical properties.

3.2.1. Equipment Selection and Description

Direct vs Bowden Extrusion System

When it comes to 3D extrusion systems, there is one major distinction. The extruder motor might be either mounted directly before the hotend (direct system) or placed further away somewhere on the printer's body (Bowden system) (Fig. 25).

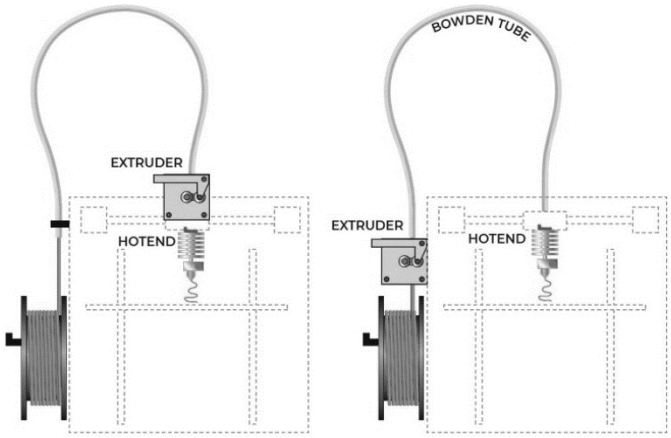

Fig. 25. Direct system (left) and Bowden system (right) [49]

The Bowden system uses a tube, which is typically made of low friction, heat resistant material like PTFE. The tube serves as a conduit for the filament and connects the extruder motor to the hotend. The main advantage of the Bowden system is that the moving carriage of the hotend can be lighter compared to the direct system, since the heavy extruder motor is fixed on the printer. This allows for faster movement and acceleration of the printing head and less vibration, due to the low mass and therefore low inertia of the moving carriage. Nevertheless, Bowden systems have certain shortcomings. Due to the long distance from the hotend, a great length of filament needs to be pushed towards the heating zone, in order to build up enough pressure. Plastics are easily deformable, resulting in the compression of the filament within the Bowden tube. A part of the extrusion force is expended on this compression, which becomes greater as the distance between the extruder and the hotend increases. Same principal applies when the filament needs to be retracted back away from the hotend. Moreover, the Bowden tube's diameter is designed with a certain tolerance, to allow the filament to glide freely through it. This free space allows the filament to buckle and compress against the tube's walls, resulting in inconsistent pressure and therefore inconsistent flowrate through the nozzle (Fig. 26). This is especially problematic with more flexible filaments (e.g. thermoplastic polyurethane) [49, 50].

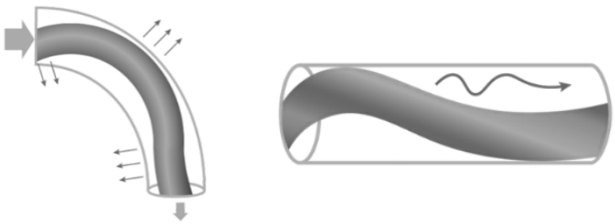

Fig. 26. Bowden tube friction (left) and buckling (right) issues [50]

In the case of the PVDF/ $BaTiO_3$ filament, it must be ensured that ideally all extrusion force is directed to increasing the nozzle pressure. Based on past experimentation, it is hypothesized that any interruption or inconsistency in the material flow can potentially accommodate nozzle clogging. Also, the PVDF filament is more flexible than the typical PLA or ABS filaments, making it prone to buckling. Another problem is that when the filament is almost expended and its end goes past the extruder motor, it is no longer possible to continue the extrusion. A length of filament slightly greater than the Bowden tube is therefore unusable and ends up as waste. These arguments necessitate the use of a direct extruder.

Nozzle Type and Diameter

The main considerations for the printing nozzle are to be abrasion resistant and allow for easy flow of the molten material. The diameter must be wider than the $BaTiO_3$ particle size. Since the $BaTiO_3$ powder used has particles of 500nm, even a 0.1mm would theoretically be enough. However, it has been observed that particles tend to agglomerate and there is a risk of high accumulation of particles in the nozzle, which in turn risks clogging it. Furthermore, the pressure required to extrude the material through a smaller orifice is greater. The most common nozzle diameter is 0.4mm. For extra safety, an even wider nozzle of 0.6mm is preferred. This nozzle should allow for a fair degree of detail, while retaining a relatively low clogging risk.

Regarding the nozzle's material, $BaTiO_3$ ceramic particles can progressively wear out nozzles made of softer materials, like brass, resulting in the uncontrolled widening of the diameter. An affordable, hard-wearing nozzle material is hardened steel. A more premium option is a nozzle fitted with a ruby tip; a material with excellent abrasion resistance, but of high cost.

3D Printer

Based on the decision for a direct extruder and a 1.75mm filament, the 3D printer options can be limited accordingly. Ease-of-use, detailed documentation, readily available community-based knowledge and customizability are the rest of the selection criteria. From a pool of available machines, the Prusa i3 MK3S+ is selected as the best option.

Slicing Software

The Slicing program or Slicer chosen is PrusaSlicer (ver. 2.4.0 for Windows 10). This piece of software is responsible for converting the .stl triangular tessellation surface model to machine toolpaths, formatted as a special code called G-code. Other options would be Cura (by Ultimaker), Simplify3D®, Slic3r (open source), etc. PrusaSlicer is developed by Prusa Research, the same supplier which manufacturs the Prusa i3 MK3S+ printer used for the experimental work. This way, excellent compatibility of the Slicer and the 3D printer is ensured. Moreover, the (as of the time of writing) most recent PrusaSlicer version offers an abundance of adjustable settings, allowing for fine and precise tuning of the 3D printing parameters.

3.2.2. Experimental Procedure

Similarly to the experiments conducted in Part 1, the 3D printing procedure is also iterative. On the hardware side, the parameters are decided during the equipment selection phase and remain unchanged throughout the experimental procedure. The most critical controlled parameters are defined in software level and the Slicing program in particular.

There are three main critical points which provide important information on the effectiveness and appropriateness of the chosen Slicing parameters and the hardware considerations (ex. adhesive type, nozzle type). The points that are evaluated are:

- the first printed layer;
- the behavior of the hotend during printing and
- the finished product.

The first layer is the foundation for the rest of the print. Therefore, monitoring of the printing of the entire first layer is mandatory. If any imperfection is observed, the print shall be interrupted. Probable issues can be bad adhesion to the build plate or under-extrusion. Intervention might be required, by immediately stopping the printing and scrapping the failed part.

Similar problems might also occur during the printing. Cooling and warpage of the 3D printed item might cause detachment from the hot bed. Partial detachment (ex. just the edges or corner features) might be acceptable, but in more extreme cases (ex. nozzle collides with printer part or part fully detaches), the part is no longer usable. Additionally, the performance of the nozzle must be monitored. It should deposit continuous strings of filament and good adhesion with the previous layers should be observed. Under-extrusion from the nozzle is an indicator of clogging. Based on these factors, the decision to continue or interrupt the process must be made, before more material is expended.

In the end, the finished part is visually inspected for obvious surface artefacts and other defects. Ideally, the surface should be smooth, the interlayer bending should be good without any signs of delamination, warping and dimensional deformation should be minimum and no discoloration of the material should be visible.

4. Experimental Results

4.1. Filament Extrusion

The final system parameters as they were determined after multiple trials are summarized in Table 5. Using an oversized die of to produce 1.75mm filament is the best option. It proved easier and more effective to control the diameter of the filament by varying the heating temperatures, the extrusion and pulling speed. Also, better roundness of the filament was observed.

The heating temperature depends on the used stock material. Manufacturer's recommendation and datasheets were used as a general guideline, to select what temperature works best for each material. The goal is for Zone 1 to fully melt the material and ensure the smooth operation of the extrusion screw. A slightly lower temperature was set for Zone 2. The reason was to control the viscosity of the molten material. Testing of equal temperatures on both heating zones revealed that the material was excessively heated, leading to low viscosity and handling difficulties.

Table 5. Extruder system parameters

Parameter	**Specification**
Die size	2.85mm
Zone 1 temperature	PLA: 180°C PVDF: 225°C
Zone 2 temperature	PLA: 170°C PVDF/ $BaTiO_3$: 235°C
Stock material form	PLA: pellets ⌀2.85mm PVDF: pellets ⌀5.65mm $BaTiO_3$: powder 500nm Fresh / Recycled
Stock material concentration	3wt% PVDF/$BaTiO_3$ 9wt% PVDF/$BaTiO_3$
Extrusion screw speed	PLA: 30RPM PVDF/$BaTiO_3$: 30RPM
Puller speed	PLA: ~5RPM PVDF/ $BaTiO_3$: 3-4.3RPM (7.8-11.25 mm/s)
Cooling method	Built-in fan: No Inline fan array: Yes Inline water bath: No

For the stock material form, the general aim was to provide continuous flow of fresh raw material of uniform size, so the extrusion mechanism can work consistently. However, in order to reduce waste, the filament can pelletized and fed again to the extruder. For the PVDF/$BaTiO_3$ filament, the filament was extruded once, then pelletized and extruded again, with the intention to achieve a better distribution of the $BaTiO_3$ particles.

The lowest $BaTiO_3$ concentration was first selected. It was considered a good starting point for the experimental work. This lower concentration should be easier to process through the extruder and the 3D printer later. As the experimentation continuous, the goal is to progressively attempt higher concentration and determine what is the maximum that can be processed by the system. 9wt% was also tested. Consistent filament could only be obtained after double extrusion.

A stable extrusion of 25 RPM was determined to be optimal. Lower speeds could not provide enough material flowrate. At higher speed setting, the actual speed was not stable and the flowrate was not consistent, because the material could not melt fast enough.

The puller speed was adjusted until the filament reached the desired diameter. Faster pulling results in thinner filament, while slower pulling results in thicker filament. PLA could be processed at slightly higher pulling speed than PVDF.

The extruder's built-in fan was turned off. If turned on, it had the tendency to blow the filament away and deform it. The inline fan array was preferred over the water bath. It provides uniform cooling of the filament and solidifies its diameter. The water bath was impractical. The electric pump provided and water flow are hard to control and the filament carries water to the puller and winder, risking water damage to the mechanical and electronic components.

Pelletizing and Double Extrusion

Pelletizing and recycling the PVDF/ $BaTiO_3$ filament greatly improved the extrusion process and the quality of the final product. The pelletizer was able to produce pellets of smaller size (<5mm in length and ~1.8mm in diameter) (Fig. 28), which did not obstruct the extrusion screw and were melted more easily. The actual extrusion screw rotational speed was constantly monitored through the extruder's display and a maximum deviation of only 1 RPM was observed, as opposed to deviation reaching 5 RPM when virgin PVDF pellets were used. Furthermore, maintaining a constant diameter without the need of continuously adjusting the pulling speed was feasible. Finally, double extruded filament featured less surface imperfections like pits or protrusions; artifacts characteristic of particle agglomeration. However, some artifacts were still visible even after recycling the material, which might be attributed to contamination from the environment (e.g. dust, debris) or the extruder itself, due to uncontrolled cleanliness conditions.

Produced Filament

A process capability analysis was conducted based on the diameter of the produced 9wt% PVDF/$BaTiO_3$ filament. A 1m long piece of filament was measured at 20mm intervals at two perpendicular directions using vernier calipers of 0.01mm accuracy. This way the geometrical consistency of the filament could be evaluated and also the capability of the extruder system. Fig. 29 shows the measurements of d1 and d2 taken at two perpendicular directions across the 1m length. The upper and lower limits are defined at 1.75 ±0.1mm. The statistical results and process capability indices are present in Table 6.

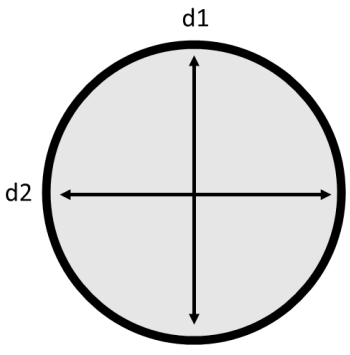

Fig. 27. Cross-sectional view of perpendicular measurements d1 and d2

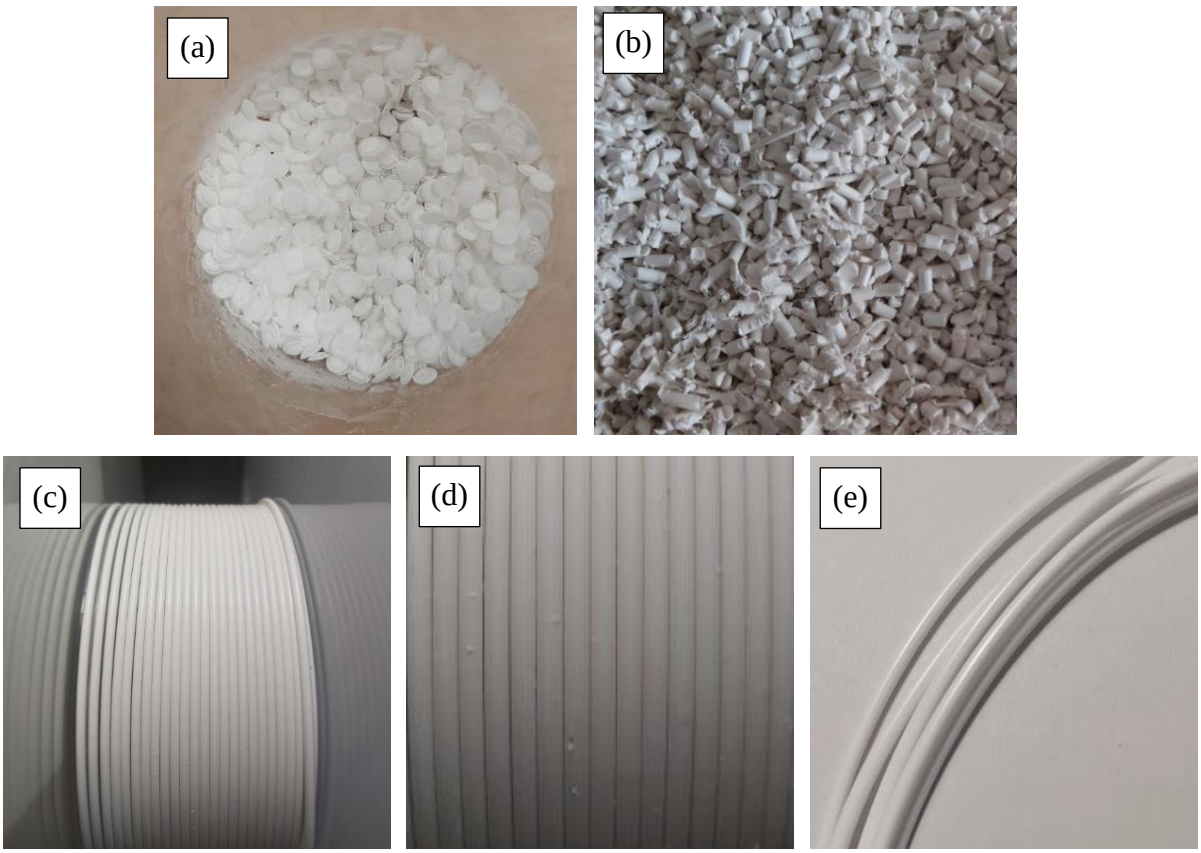

Fig. 28. Pure PVDF/$BaTiO_3$ stock material (a), pelletized PVDF/$BaTiO_3$ filament (b), once extruded 9wt% PVDF/$BaTiO_3$ filament and detail of surface artifacts (c and d), double-extruded 9wt% PVDF/$BaTiO_3$ filament (e)

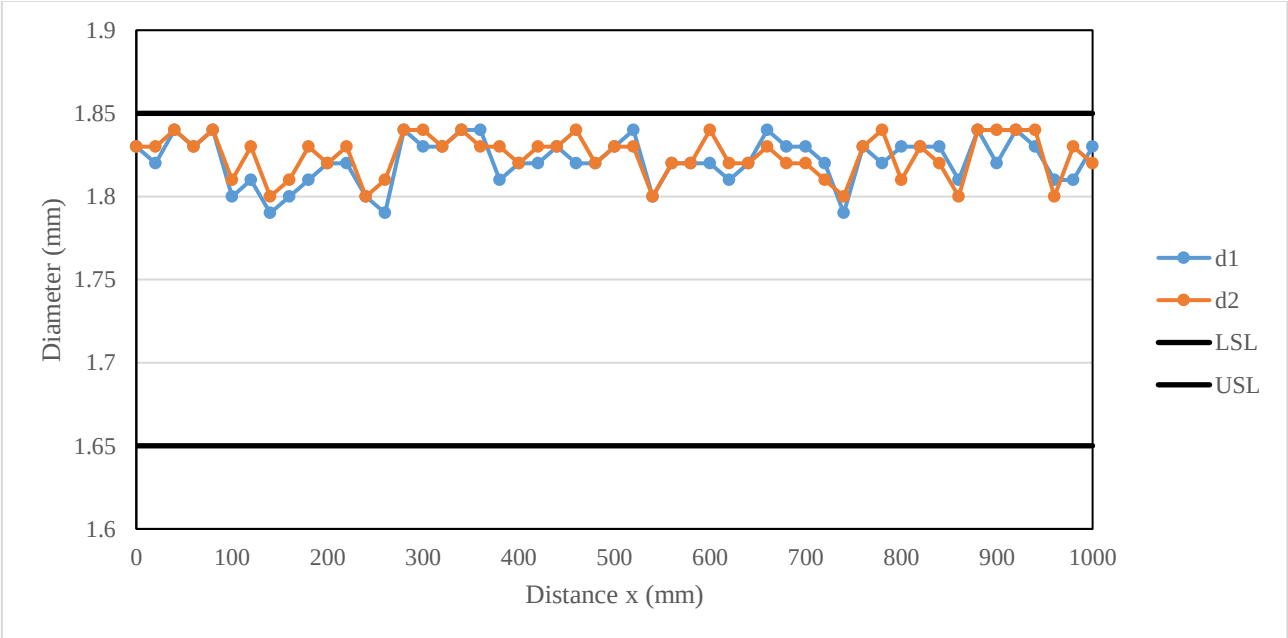

Fig. 29. Diameter VS distance of 9wt% PVDF/$BaTiO_3$ filament

Table 6. Process capability results of 9wt% double-extruded PVDF/$BaTiO_3$ filament

	d1	**d2**
Min	1.79	1.8
Max	1.84	1.84
Mean	1.82	1.82
Median	1.82	1.83
Standard Deviation σ	0.014053	0.012861
Coefficient of variation CV	0.007715	0.007048
Cp	2.37	2.59
CpL	4.07	4.53
CpU	0.67	0.66
Cpk	0.67	0.66

4.2. FDM 3D printing

Tests on the 3D printer yielded a 4-layer ISO 527-2B specimen with a height of 0.8mm. The best medium for improving bed adhesion was determined to be Dimafix liquid adhesive, further aided by a 5mm brim, a heated bed at 105°C and no cooling. Printing temperature of 250°C was used, as lower temperatures could not induce satisfactory interlayer bonding, with the extruded material tending to curl away from the underlying structure. Printing speed was constant for all printing features and it was selected at 10 mm/s, while retractions were disabled. Higher speeds and retractions resulted in breaking of the extruded threads of material and inconsistent deposition on the surface. The FDM parameters are summarized in Table 7. For the full Slicing parameters and configured in PrusaSlicer 2.4.0. refer to the Appendix 2.

The pure PVDF sample was qualitatively evaluated. First attempts with lower heating and higher speed settings yielded poor results. The extrudate was not able to bond well to neighboring structures and it formed lumbs of detached material. With optimized printing parameters, minor delamination from the build surface was observed on the brim perimeters (Fig. 30). At certain areas, burn marks were visible, but it was theorized that they were due to residual material from previous printing process on nozzle (Fig. 30). Accumulation of residual material was still seen on both the printing nozzle and the printed layers, but at a lesser degree (Fig. 31). This was evidence of over-extrusion or excessive overlap of the printed lines.

Fig. 30. 4-layer PVDF specimen with signs of build plate detachment and burning

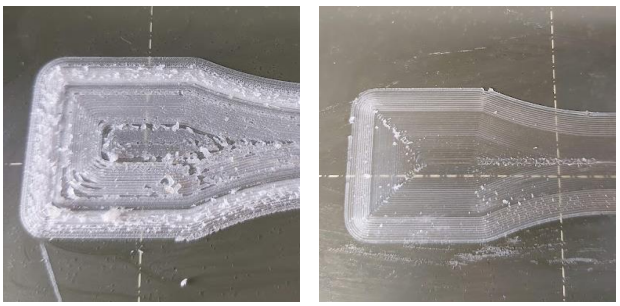

Fig. 31. 3D printed PVDF sample before (left) and after (right) optimizing FDM parameters

Table 7. 3D printing parameters for pure PVDF filament

Parameter	**Specification**
Slicer	PrusaSlicer 2.4.0 W10
3D printer	Prusa i3 MK3S+
Extrusion system	Direct
Nozzle type	Brass / Hardened steel
Nozzle diameter	0.4mm
Nozzle temperature	250
Hotbed temperature	105
Layer height	0.2mm
Speed	10mm/s
Infill percentage	n/a
Infill pattern	n/a
Perimeter count	50
Printing sequence	External first
Brim	5mm width
Bed adhesion	Dimafix liquid
Cooling	n/a
Retraction	n/a
Surface type	Prusa default

9wt% PVDF/$BaTiO_3$ was also tested using the same process parameters. However, a specimen could not be printed, due to under-extrusion. The extruder was unable to push the filament through the hotend, which resulted in inconsistent extrusion flow through the default 0.4mm brass nozzle. Artifacts were later observed on the filament, which indicated that the material remained stationary and the extruder gear was grinding the material.

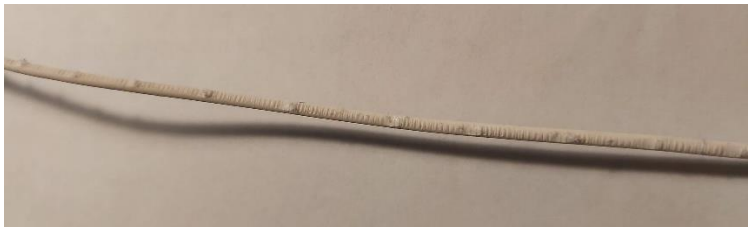

Fig. 32. 9wt% PVDF/$BaTiO_3$ filament after feeding to 3D printer extruder

Conclusions

The investigation of PVDF/$BaTiO_3$ composite 3D printing material revealed that it is feasible to fabricate filament with dimensional accuracy comparable to common, commercially available products. Compared to typical PLA 3D printing material, the raw materials proved more challenging to process using hot extrusion. Increased melt temperature, decreased extrusion speed and re-palletization were required to establish a stable flow of material through the system. Furthermore, stable dimensions could only be achieved by using an oversized extruder die. Increased static attraction of foreign particles was observed, which could potentially compromise the purity of the final product.

1. PVDF 3D printing material with $BaTiO_3$ particles was succesfully produced. The target dimensional accuracy of 1.75mm ±0.1mm was achieved. For this purpose, a desktop filament extruder was used, alongside a cooling fan array and pulling mechanism. The pulling mechanism was an important consideration and its control electronics were improved to achieve fine and precise control. Optimal pulling speed was determined to be in the range of 7.8-11.25 mm/s. Extruder temperature was determined to be 225°C at Zone 1 and 235°C at Zone 2, while constant extrusion speed of 25RPM was maintained. Furthermore, peletizing the produced filament and feeding it back to the extruder (double extrusion) helped maintain a stable extrusion process and reduced surface imperfections observed on the filament.
2. The main quality parameters of the produced filament and its fabrication procedure were determined by statistically analysing the diameter of the finished product. An 1m 9wt% PVDF/ $BaTiO_3$ filament sample was used and measurements taken at regular intervals. The maximum diameter variance was 0.05mm, Cp value was 2.59 and Cpk value was 0.67. The low Cpk value indicates that the process is not capable, however it should be considered that this is due to limits defined in the beginning of the process capability analysi, which resulted in non-centered measurements. In practice, this is not a major problem for 3D printing, because provided that the diameters is reasonable stable, any deviation from the optimal 1.75mm can be compensated in the slicing software.
3. The 3D printing properties were evaluated and the main parameters were identified. Provisions for good build plate adhesion, slow printing speed of 10 mm/s and nozzle temperature at 250°C yielded the best results. Moreover, with the optimization of the printing parameters and iterative testing, interlayer bonding and surface finish were significantly improved. A 0.4mm nozzle was sufficient for printing pure PVDF filament, however clogging was observed when the PVDF/$BaTiO_3$ filament was introduced.

Recommendations

There is a number of considerations which could potentially improve the results yielded by the procedures mentioned in this paper and also help with the evaluation of the finished product.

Regarding the extrusion process itself, it was made evident that better cleanliness control is mandatory. Especially in the case of double extrusion, the material has a second chance of collecting foreign contaminates, which will eventually be included in the finished filament product. A thorough cleaning step of the filament before pelletizing it is advised. Also, cleaning of the pulling and winding equipment and materials is also necessary to prevent the accumulation of dust. For the prevention of statically attracted particles, air ionizing devices might also be utilized.

For the 3D printing process, the main improvement would be the replacement of the default printing nozzle with one of larger diameter. A 0.6mm or 0.8mm nozzle should allow for better flowrate and be less susceptible to clogging due to $BaTiO_3$ particle agglomeration.

For the characterization of the specimens' morphology more in-depth techniques should be employed. Cross sectional SEM views of the produced filament could reveal and imperfections like porosities and also help evaluate how well the $BaTiO_3$ particles are distributed. Comperative FTIR spectra of the produced filament with and without the pulling mechanism could show whether stretching of the filament has any effect on the β-phase content. For the mechanical characterization, smaller tensile strength specimens should be considered (e.g. ISO 527-1BA or ISO 527-1BB), which are more probable to be fully 3D printed.

List of references

1. CARDOSO, V.F., et al. Fluorinated Polymers as Smart Materials for Advanced Biomedical Applications. *Polymers*, vol. 10, 2018, no. 2. pp. 161 [viewed Feb, 2022] ISSN 2073-4360. DOI 10.3390/polym10020161.
2. KHOSRAVANI, M.R. & REINICKE, T. 3D-Printed Sensors: Current Progress and Future Challenges. *Sensors and Actuators.A.Physical.*, vol. 305, 2020. pp. 111916 [viewed Mar, 2022] ISSN 0924-4247. DOI 10.1016/j.sna.2020.111916.
3. KIM, H., et al. Integrated 3D Printing and Corona Poling Process of PVDF Piezoelectric Films for Pressure Sensor Application. *Smart Materials and Structures*, vol. 26, 2017, no. 8. pp. 85027 [viewed Mar, 2022] ISSN 0964-1726. DOI 10.1088/1361-665X/aa738e.
4. MULLAVEETTIL, F.N., et al. Development of Electroactive PVDF Films by using 3D Printing and Contact Poling. *Mechanika 2018: Proceedings of the 23rd International Scientific Conference, 18 may 2018, Kaunas University of Technology, Lithuania*, 2018. pp. 113-117 [viewed Feb, 2022] ISSN 1822-2951.
5. Clarivate. *Web of Science.* [viewed Mar, 2022]. Available from: https://www.webofscience.com/wos/woscc/basic-search.
6. KIM, H., et al. 3D Printing of BaTiO3/PVDF Composites with Electric in Situ Poling for Pressure Sensor Applications. *Macromolecular Materials and Engineering*, vol. 302, 2017, no. 11. pp. n/a [viewed Feb, 2022] ISSN 1438-7492. DOI 10.1002/mame.201700229.
7. LI, Y., et al. Multi-Layered BTO/PVDF Nanogenerator with Highly Enhanced Performance Induced by Interlaminar Electric Field. *Microelectronic Engineering*, vol. 244-246, 2021. pp. 111557 [viewed Mar, 2022] ISSN 0167-9317. DOI 10.1016/j.mee.2021.111557.
8. SHARMA, R. Study on Barium Titanate and Graphene Reinforced PVDF Matrix for 4D Applications. *Journal of Thermoplastic Composite Materials*, vol. 34, 2021, no. 9. pp. 1234-1254 [viewed Mar, 2022] ISSN 0892-7057. DOI 10.1177/0892705719865004.
9. PHATHARAPEETRANUN, N., et al. 3D-Printed Barium Titanate/Poly-(Vinylidene Fluoride) Nano-Hybrids with Anisotropic Dielectric Properties. *Journal of Materials Chemistry.C, Materials for Optical and Electronic Devices*, vol. 5, 2017, no. 47. pp. 1243-1244 [viewed Feb, 2022] ISSN 2050-7526. DOI 10.1039/c7tc03697c.
10. MULLAVEETTIL, F.N., DAUKSEVICIUS, R., RIMASAUSKAS, M. & GRIGALIUNAS, V. Fused Filament Fabrication and Mechanical Performance of PVDF-Based Specialty Thermoplastics. *International Journal of Advanced Manufacturing Technology*, vol. 117, 2021, no. 11-12. pp. 3267-3280 [viewed Feb, 2022] ISSN 0268-3768. DOI 10.1007/s00170-021-07887-6.
11. Arkema. *Kynar-Pvdf-Performance-Characteristics-Data-Brochure.* , 2020 [viewed Apr 2022]. Available from: https://www.arkema.com/global/en/products/product-finder/product-range/technicalpolymers/kynar-product-family/.
12. Solvay. *Solef ® PVDF Design & Processing Guide Solef ®.* , Nov, 2019 [viewed Apr 2022]. Available from: https://www.solvay.com/en/brands/solef-pvdf/documents.
13. CARDOSO, V.F., et al. *Fluorinated Polymers as Smart Materials for Advanced Biomedical Applications.* , 2018 ISBN 2073-4360. Available from: 10.3390/polym10020161.

14. AMEDURI, B. & SAWADA, H. *Fluorinated Polymers.* The Royal Society of Chemistry, 2017 Available from: http://dx.doi.org/10.1039/9781782629368 ISBN 978-1-78262-916-0. DOI 10.1039/9781782629368.
15. J. DROBNY. *Properties of Polyvinyl Fluoride: Datasheet from Landolt-Börnstein - Group VIII Advanced Materials and Technologies · Volume 13: "Specialty Thermoplastics" in SpringerMaterials (Https://Doi.Org/10.1007/978-3-662-46419-9_8).* J. DROBNY ed., Springer-Verlag Berlin Heidelberg. Available from: https://materials.springer.com/lb/docs/sm_lbs_978-3-662-46419-9_8 DOI 10.1007/978-3-662-46419-9_8.
16. MISHRA, S., UNNIKRISHNAN, L., NAYAK, S.K. & MOHANTY, S. Advances in Piezoelectric Polymer Composites for Energy Harvesting Applications: A Systematic Review. *Macromolecular Materials and Engineering*, vol. 304, 2019, no. 1. pp. 1800463. Available from: https://doi.org/10.1002/mame.201800463 ISSN 1438-7492. DOI https://doi.org/10.1002/mame.201800463.
17. Arkema Inc. *PERFORMANCE CHARACTERISTICS & DATA Kynar ® PVDF*. , 2020 Available from: https://hpp.arkema.com/en/product-families/kynar-fluoropolymer-family/download-performance-characteris/.
18. James Henry, Averie Palovcak and Skip Sparks. *Kynar® PVDF Injection Molding -Standard Guidelines and New Technologies.* , May, 2022 Available from: https://hpp.arkema.com/en/product-families/kynar-fluoropolymer-family/processing-guidelines/injection-molding-white-paper-download/.
19. YIN, Z., TIAN, B., ZHU, Q. & DUAN, C. Characterization and Application of PVDF and its Copolymer Films Prepared by Spin-Coating and Langmuir-Blodgett Method. *Polymers*, vol. 11, 2019, no. 12. pp. 2033 ISSN 2073-4360. DOI 10.3390/polym11122033.
20. RIBEIRO, C., et al. Electroactive Poly(Vinylidene Fluoride)-Based Structures for Advanced Applications. *Nature Protocols*, vol. 13, 2018, no. 4. pp. 681-704. Available from: https://doi.org/10.1038/nprot.2017.157 ISSN 1750-2799. DOI 10.1038/nprot.2017.157.
21. GREESHMA, T., BALAJI, R. & JAYAKUMAR, S. PVDF Phase Formation and its Influence on Electrical and Structural Properties of PZT-PVDF Composites. *Ferroelectrics.Letters Section*, vol. 40, 2013, no. 1-3. pp. 41-55 ISSN 0731-5171. DOI 10.1080/07315171.2013.814460.
22. TIWARI, V. & SRIVASTAVA, G. Structural, Dielectric and Piezoelectric Properties of 0–3 PZT/PVDF Composites. *Ceramics International*, vol. 41, 2015, no. 6. pp. 8008-8013. Available from: https://www.sciencedirect.com/science/article/pii/S0272884215003892 ISSN 0272-8842. DOI https://doi.org/10.1016/j.ceramint.2015.02.148.
23. LI, R., ZHAO, Z., CHEN, Z. & PEI, J. Novel BaTiO 3 /PVDF Composites with Enhanced Electrical Properties Modified by Calcined BaTiO 3 Ceramic Powders. *Materials Express*, vol. 7, 2017. pp. 536-540 DOI 10.1166/mex.2017.1393.
24. BATRA, A., EDWARDS, M., ALOMARI, A. & ELKHALDY, A. Dielectric Behavior of P(VDF-TrFE) /PZT Nanocomposites Films Doped with Multi-Walled Carbon Nanotubes (MWCNT). *American Journal of Materials Science*, vol. 2015, 2015. pp. 55-61 DOI 10.5923/s.materials.201502.09.
25. KIM, J., LOH, K.J. and LYNCH, J.P. *Proceedings of SPIE*. Bellingham, Wash: Bellingham, Wash: SPIE, 2008 ISBN 0277-786X. Available from: 10.1117/12.774256.
26. PUSTY, M., et al. Comparative Study with a Unique Arrangement to Tap Piezoelectric Output to Realize a Self Poled PVDF Based Nanocomposite for Energy Harvesting Applications.

ChemistrySelect, vol. 2, 2017, no. 9. pp. 2774-2782. Available from: https://doi.org/10.1002/slct.201602046 ISSN 2365-6549. DOI https://doi.org/10.1002/slct.201602046.

27. CHEN, H., et al. Investigation of PVDF-TrFE Composite with Nanofillers for Sensitivity Improvement. *Sensors and Actuators A: Physical*, vol. 245, 2016. pp. 135-139. Available from: https://www.sciencedirect.com/science/article/pii/S0924424716302011 ISSN 0924-4247. DOI https://doi.org/10.1016/j.sna.2016.04.056.
28. TAMANG, A., et al. DNA-Assisted B-Phase Nucleation and Alignment of Molecular Dipoles in PVDF Film: A Realization of Self-Poled Bioinspired Flexible Polymer Nanogenerator for Portable Electronic Devices. *ACS Applied Materials & Interfaces*, vol. 7, 2015, no. 30. pp. 16143-16147 ISSN 1944-8244. DOI 10.1021/acsami.5b04161.
29. ROY, S., et al. Electroactive and High Dielectric Folic Acid/PVDF Composite Film Rooted Simplistic Organic Photovoltaic Self-Charging Energy Storage Cell with Superior Energy Density and Storage Capability. *ACS Applied Materials & Interfaces*, vol. 9, 2017, no. 28. pp. 24198-24209. Available from: https://doi.org/10.1021/acsami.7b05540 ISSN 1944-8244. DOI 10.1021/acsami.7b05540.
30. CHEN, C., et al. 3D Printing of Electroactive PVDF Thin Films with High B-Phase Content. *Smart Materials and Structures*, vol. 28, 2019, no. 6. pp. 65017 ISSN 0964-1726. DOI 10.1088/1361-665X/ab15b7.
31. LEE, C. & TARBUTTON, J.A. Electric Poling-Assisted Additive Manufacturing Process for PVDF Polymer-Based Piezoelectric Device Applications. *Smart Materials and Structures*, vol. 23, 2014, no. 9. pp. 1-7 ISSN 0964-1726. DOI 10.1088/0964-1726/23/9/095044.
32. KIM, H., et al. Enhanced Dielectric Properties of Three Phase Dielectric MWCNTs/BaTiO3/PVDF Nanocomposites for Energy Storage using Fused Deposition Modeling 3D Printing. *Ceramics International*, vol. 44, 2018, no. 8. pp. 9037-9044. Available from: https://www.sciencedirect.com/science/article/pii/S0272884218304048 ISSN 0272-8842. DOI https://doi.org/10.1016/j.ceramint.2018.02.107.
33. ZHANG, Z., et al. Aberrant Expression of miRNA-192-5p Contributes to N,N-dimethylformamide-induced Hepatic Apoptosis. *Journal of Applied Toxicology*, vol. 40, 2020, no. 12. pp. 1683-1693 ISSN 0260-437X. DOI 10.1002/jat.4028.
34. MOMENZADEH, N., MIYANAJI, H., PORTER, D.A. & BERFIELD, T.A. Polyvinylidene Fluoride (PVDF) as a Feedstock for Material Extrusion Additive Manufacturing. *Rapid Prototyping Journal*, vol. 26, 2020, no. 1. pp. 156-163 ISSN 1355-2546. DOI 10.1108/RPJ-08-2018-0203.
35. FARINA, I., et al. Mechanical Characterization of FDM Filaments with PVDF Matrix Reinforced with Graphene and Barium Titanate. *IOP Conference Series: Materials Science and Engineering*, vol. 999, 2020. pp. 012010 DOI 10.1088/1757-899X/999/1/012010.
36. LIU, W., et al. Fabrication of PLA Filaments and its Printable Performance. *IOP Conference Series.Materials Science and Engineering*, vol. 275, 2017, no. 1. pp. 12033 ISSN 1757-8981. DOI 10.1088/1757-899X/275/1/012033.
37. *New FluorX PVDF-C MAX 3D Printing Filament, by 3DXTECH*. [viewed May 2022]. Available from: https://www.3dxtech.com/product/fluorx-pvdf-c-max/.
38. *Fluorodur 1.75 Mm*. [viewed May 2022]. Available from: https://www.3djake.com/fillamentum/fluorodur.

39. Boots Industries. *The Importance of High Quality 3D Printer Filament – Boots Industries.* [viewed Apr 2022]. Available from: http://bootsindustries.com/the-importance-of-high-quality-3d-printer-filament/.
40. MULLAVEETTIL, F.N., DAUKSEVICIUS, R. & WAKJIRA, Y. Strength and Elastic Properties of 3D Printed PVDF-Based Parts for Lightweight Biomedical Applications. *Journal of the Mechanical Behavior of Biomedical Materials*, vol. 120, 2021. pp. 104603. Available from: https://www.sciencedirect.com/science/article/pii/S175161612100285X ISSN 1751-6161. DOI https://doi.org/10.1016/j.jmbbm.2021.104603.
41. KIM, H. Fabrication and Characterization of 3D Printed BaTiO/PVDF Nanocomposites. *Journal of Composite Materials*, vol. 52, 2018, no. 2. pp. 197-207 [viewed Nov 2021] ISSN 0021-9983. DOI 10.1177/0021998317704709.
42. *Downloads | FormFutura.* [viewed May 2022]. Available from: http://www.formfutura.com/downloads.
43. *Poly(Vinylidene Fluoride-Co-Hexafluoropropylene) Average Mw 400,000, Average Mn 130,000, Pellets 9011-17-0.* [viewed May 2022]. Available from: http://www.sigmaaldrich.com/.
44. Noztek. *Noztek Touch & Noztek Touch HT Desktop 3D Filament Extruder*. [viewed Apr 2022]. Available from: https://www.noztek.com/product/noztek-touch/.
45. Wellzoom. *Wellzoom 2021 Models Desktop Extruder Line II+ （450℃） – Wellzoom.* [viewed Apr 2022]. Available from: http://wellzoomextruder.com/product/wellzoom-desktop-extruder-line-ii-%ef%bc%88450%e2%84%83%ef%bc%89/.
46. *Pololu - A4988 Stepper Motor Driver Carrier.* [viewed May 2022]. Available from: https://www.pololu.com/product/1182.
47. Texas Instruments. *LM555 Timer.* , Feb, 2000 [viewed May 2022]. Available from: https://www.ti.com/lit/ds/symlink/lm555.pdf.
48. *Tmc2208-La.* [viewed May 2022]. Available from: https://www.trinamic.com/products/integrated-circuits/details/tmc2208-la/.
49. Recreus. *Direct Extrusion Vs. Bowden Type -.* [viewed Apr 2022]. Available from: https://recreus.com/gb/noticias/learn-with-recreus/direct-extrusion-vs-bowden-type.
50. E3D. *Battling Bowden Tube Physics.* [viewed Apr 2022]. Available from: https://e3d-online.com/blogs/news/battling-bowden-tube-physics.

Appendices

Appendix 1. Computer code

Control code for puller system in C language:

```
1  // Define pin connections & motor's steps per revolution
2  const int dirPin = 2;
3  const int stepPin = 3;
4  const int stepsPerRevolution = 200;
5  const int potPin = A0;
6  int period;
7  int pot;
8  int min_period = 50;
9  int max_period = 2000;
10
11 void setup()
12 {
13   Serial.begin(9600);
14   // Declare pins as Outputs
15   pinMode(stepPin, OUTPUT);
16   pinMode(dirPin, OUTPUT);
17   // Set motor direction clockwise
18   digitalWrite(dirPin, HIGH);
19   period = min_period;
20 }
21 void loop(){
22     period=min_period + (max_period-min_period)/1023*analogRead(potPin);
23
24     digitalWrite(stepPin, HIGH);
25     delayMicroseconds(period);
26     digitalWrite(stepPin, LOW);
27     delayMicroseconds(period);
28 }
```

Appendix 2. Slicer settings

Views from the PrusaSlicer with detailed Slicing settings:

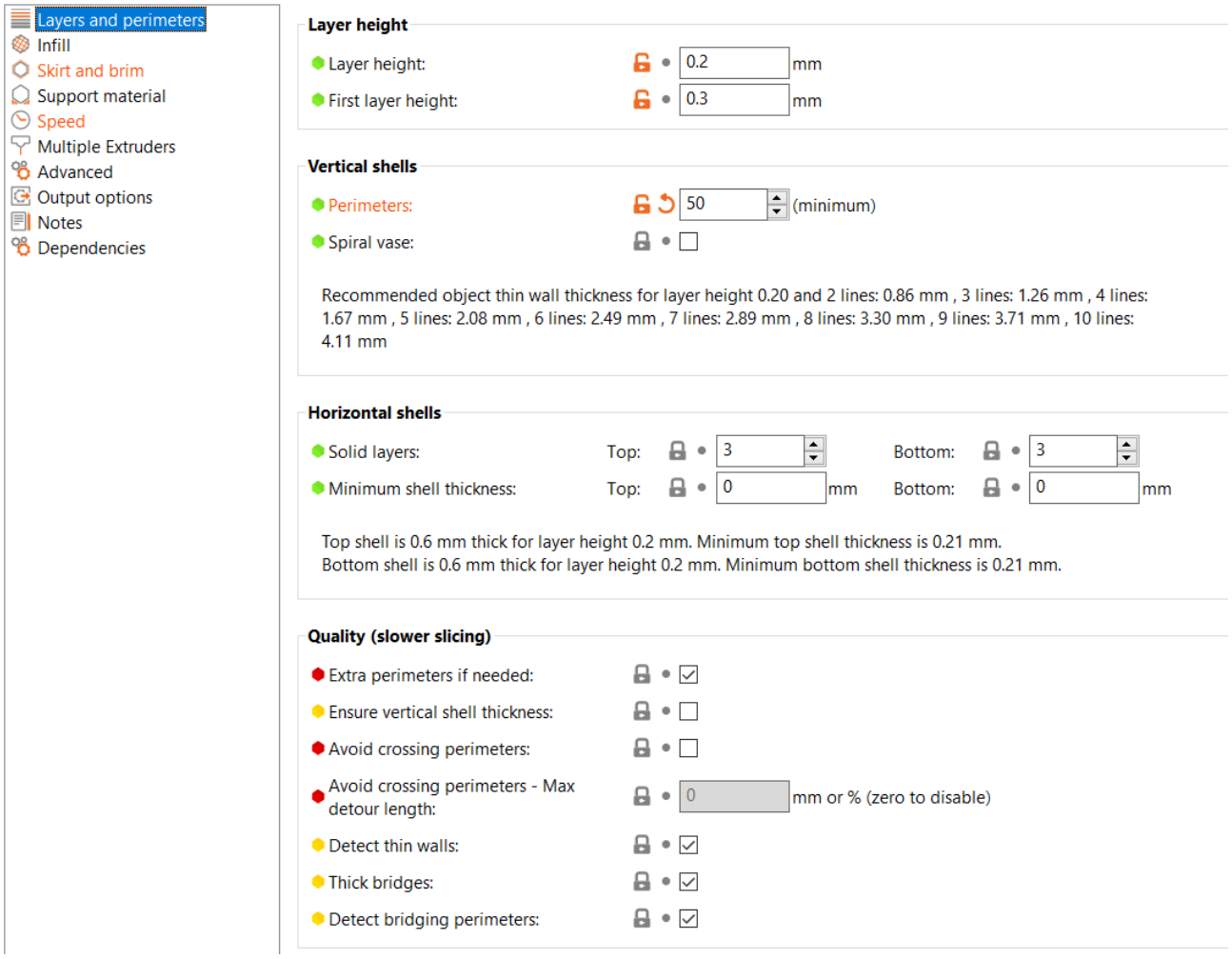

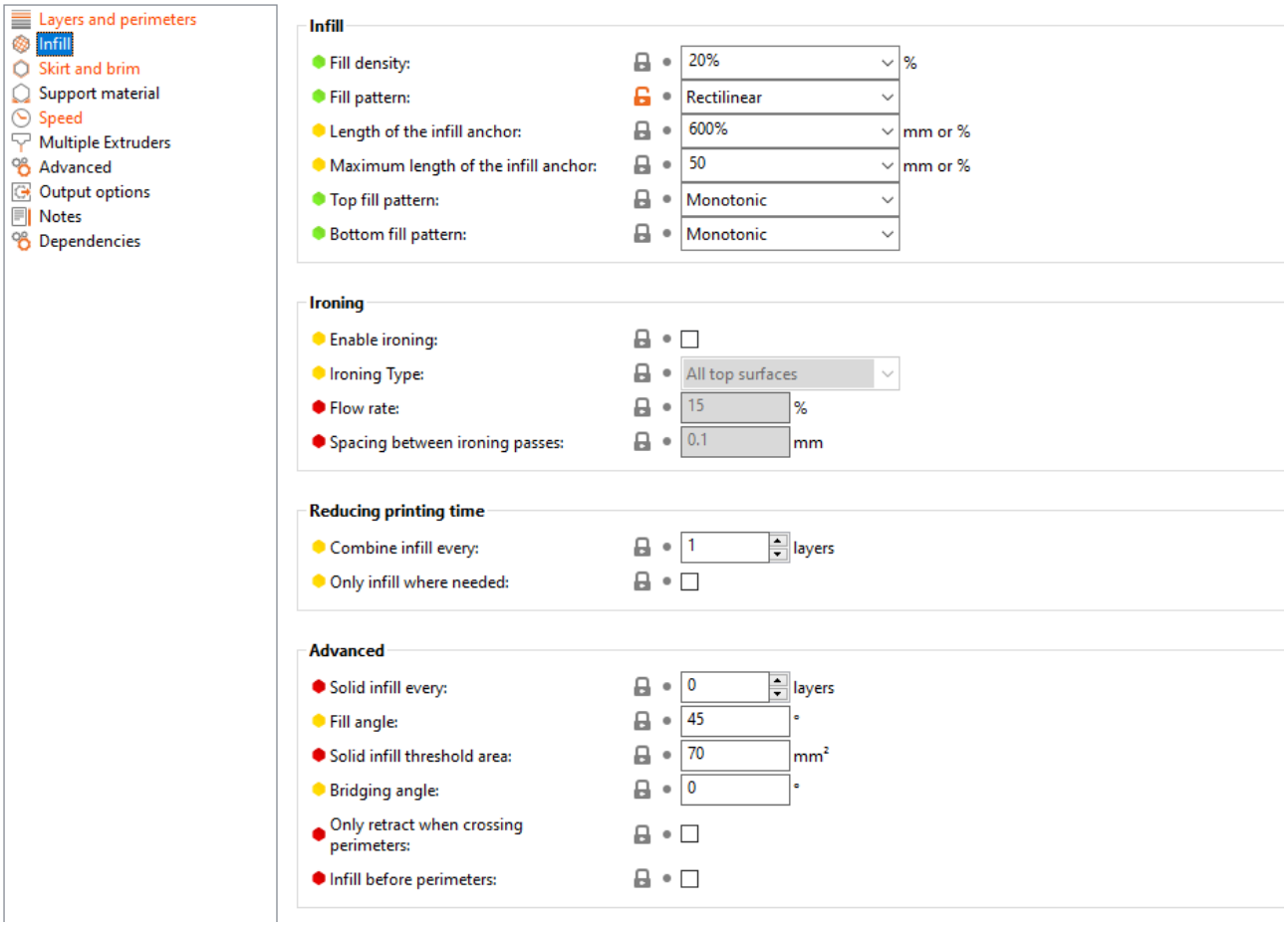
Layers and perimeters
Infill
Skirt and brim
Support material
Speed
Multiple Extruders
Advanced
Output options
Notes
Dependencies
Infill
Fill density: 20% %
Fill pattern: Rectilinear
Length of the infill anchor: 600% mm or %
Maximum length of the infill anchor: 50 mm or %
Top fill pattern: Monotonic
Bottom fill pattern: Monotonic
Ironing
Enable ironing:
Ironing Type: All top surfaces
Flow rate: 15 %
Spacing between ironing passes: 0.1 mm
Reducing printing time
Combine infill every: 1 layers
Only infill where needed:
Advanced
Solid infill every: 0 layers
Fill angle: 45 °
Solid infill threshold area: 70 mm²
Bridging angle: 0 °
Only retract when crossing perimeters:
Infill before perimeters:

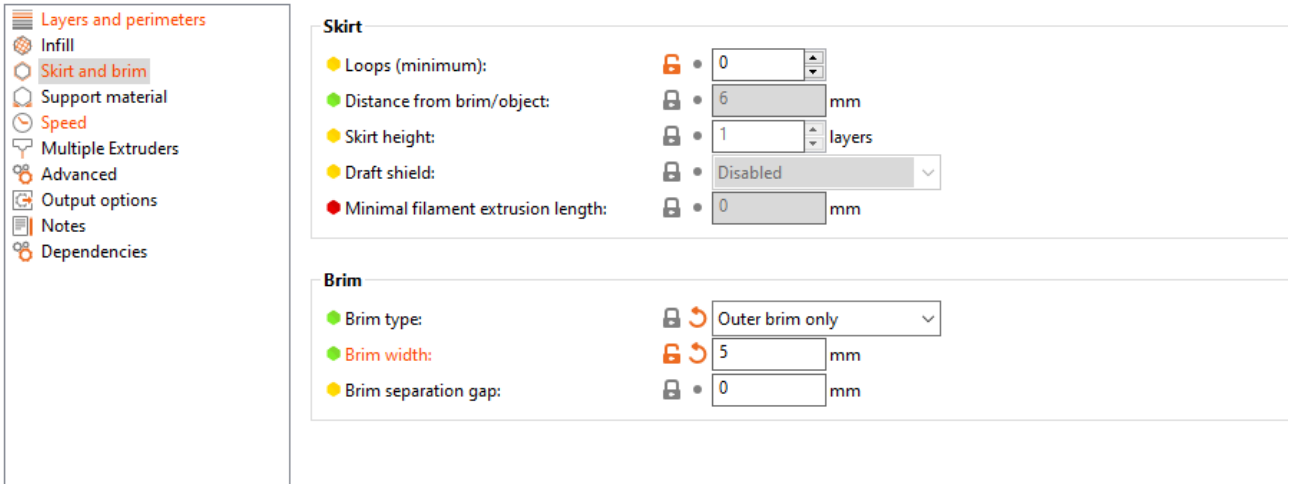
Layers and perimeters
Infill
Skirt and brim
Support material
Speed
Multiple Extruders
Advanced
Output options
Notes
Dependencies
Skirt
Loops (minimum): 0
Distance from brim/object: 6 mm
Skirt height: 1 layers
Draft shield: Disabled
Minimal filament extrusion length: 0 mm
Brim
Brim type: Outer brim only
Brim width: 5 mm
Brim separation gap: 0 mm

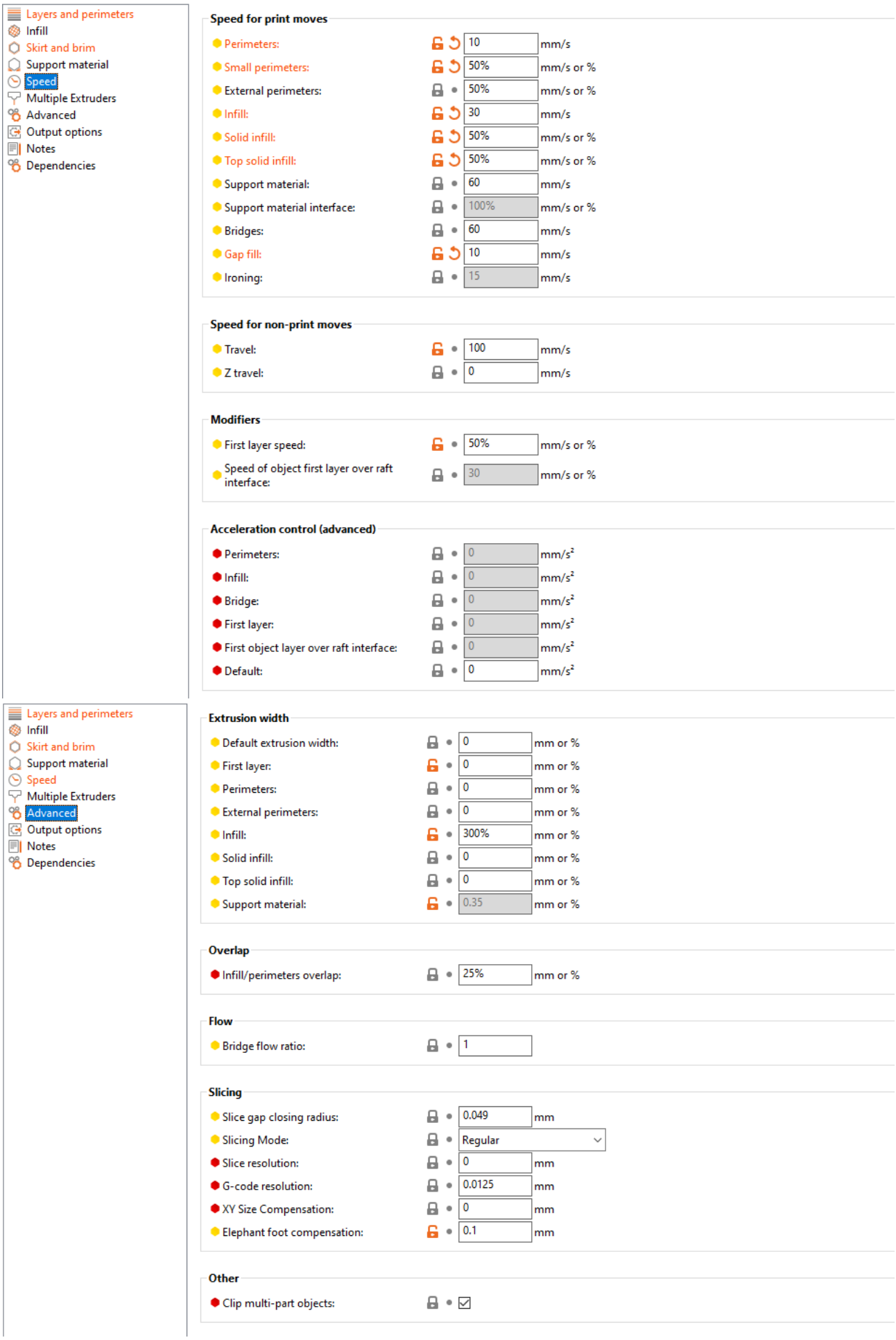
Layers and perimeters
Infill
Skirt and brim
Support material
Speed
Multiple Extruders
Advanced
Output options
Notes
Dependencies
Speed for print moves
Perimeters: 10 mm/s
Small perimeters: 50% mm/s or %
External perimeters: 50% mm/s or %
Infill: 30 mm/s
Solid infill: 50% mm/s or %
Top solid infill: 50% mm/s or %
Support material: 60 mm/s
Support material interface: 100% mm/s or %
Bridges: 60 mm/s
Gap fill: 10 mm/s
Ironing: 15 mm/s
Speed for non-print moves
Travel: 100 mm/s
Z travel: 0 mm/s
Modifiers
First layer speed: 50% mm/s or %
Speed of object first layer over raft interface: 30 mm/s or %
Acceleration control (advanced)
Perimeters: 0 mm/s²
Infill: 0 mm/s²
Bridge: 0 mm/s²
First layer: 0 mm/s²
First object layer over raft interface: 0 mm/s²
Default: 0 mm/s²
Layers and perimeters
Infill
Skirt and brim
Support material
Speed
Multiple Extruders
Advanced
Output options
Notes
Dependencies
Extrusion width
Default extrusion width: 0 mm or %
First layer: 0 mm or %
Perimeters: 0 mm or %
External perimeters: 0 mm or %
Infill: 300% mm or %
Solid infill: 0 mm or %
Top solid infill: 0 mm or %
Support material: 0.35 mm or %
Overlap
Infill/perimeters overlap: 25% mm or %
Flow
Bridge flow ratio: 1
Slicing
Slice gap closing radius: 0.049 mm
Slicing Mode: Regular
Slice resolution: 0 mm
G-code resolution: 0.0125 mm
XY Size Compensation: 0 mm
Elephant foot compensation: 0.1 mm
Other
Clip multi-part objects:

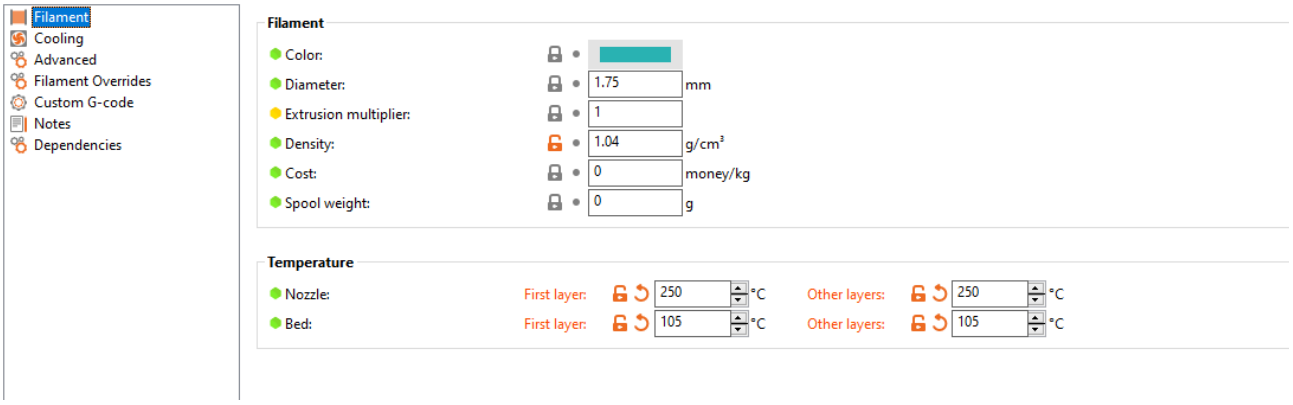

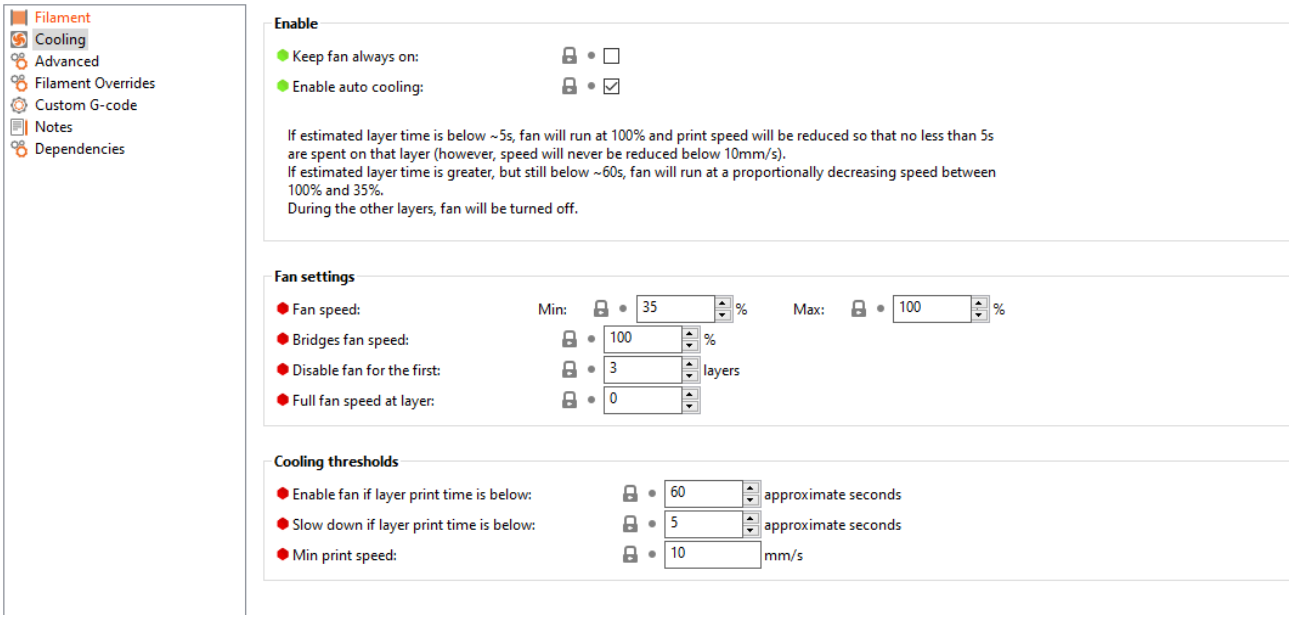

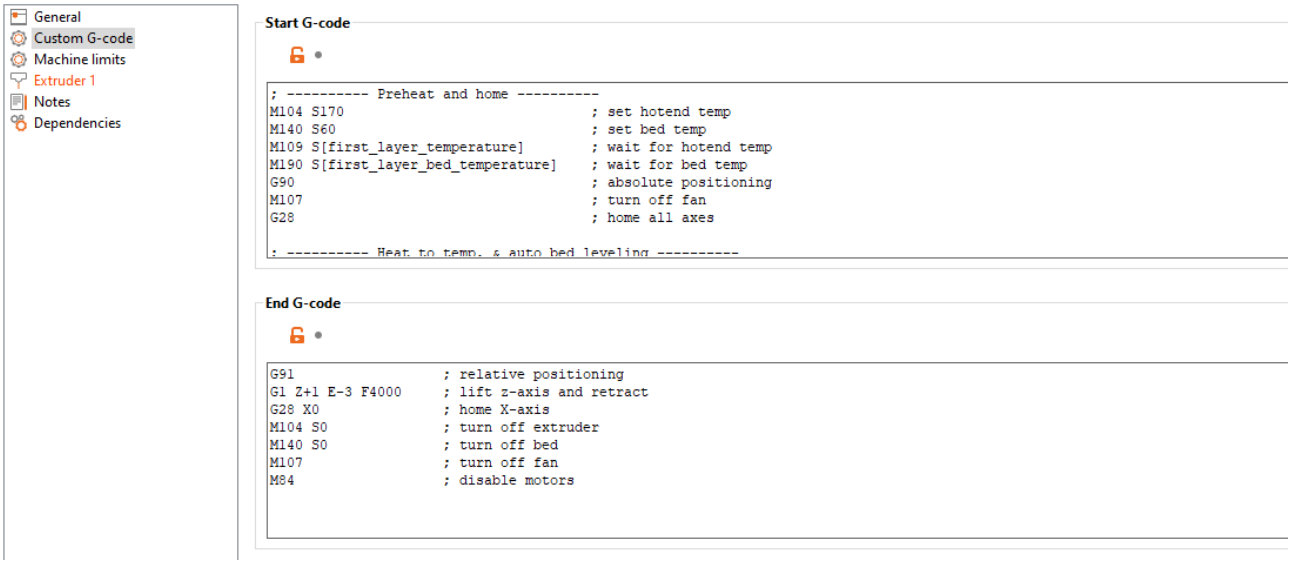

Start G-Code:

1	; ---------- Preheat and home ----------	
2	M104 S170	; set hotend temp
3	M140 S60	; set bed temp
4	M109 S[first_layer_temperature]	; wait for hotend temp
5	M190 S[first_layer_bed_temperature]	; wait for bed temp

6	G90
7	M107
8	G28
9	
10	; ---------- Heat to temp. & auto bed leveling ----------
11	M104 S[first_layer_temperature] ; set hotend temp
12	M140 S[first_layer_bed_temperature] ; set bed temp
13	G29
14	
15	; ---------- Purge line ----------
16	G0 X10 Y10 F5000
17	G0 Z0.15
18	G92 E0
19	G1 X40 E35 F500
20	G92 E0
21	G1 E-1 F500
22	G1 X70 F4000
23	G1 Z0.3